iScience

Article

A design principle for neuronal firing with up-down oscillation through Na^+ dynamics

Graphical abstract

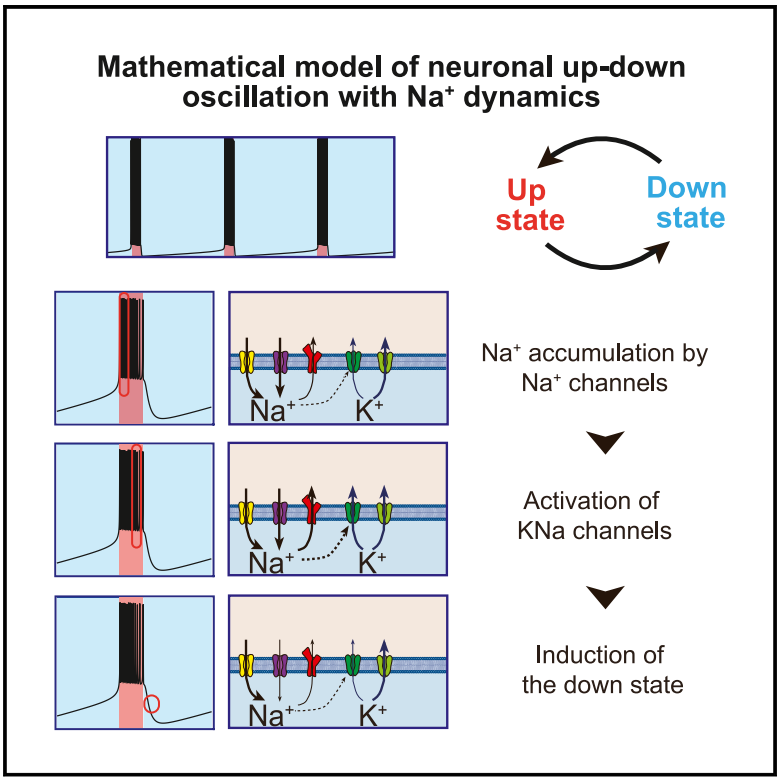

Authors

Tomohide R. Sato, Koji L. Ode, Fukuaki L. Kinoshita, Hiroki R. Ueda

Correspondence

uedah-tky@umin.ac.jp

In brief

Neuroscience; Cell biology; Mathematical biosciences

Highlights

- A Hodgkin-Huxley-type model focusing on neuronal Na^+ dynamics is developed
- Sleep-related neuronal firing with alternating up and down states is simulated
- Na^+-dependent hyperpolarization pathway recapitulates up-down oscillation
- Voltage sensitivity of voltage-gated Na^+ channels is crucial for up-down oscillation

Sato et al., 2025, iScience *28*, 111904
February 21, 2025
https://doi.org/10.1016/j.isci.2025.111904

CellPress

iScience

CellPress
OPEN ACCESS

Article

A design principle for neuronal firing with up-down oscillation through Na^+ dynamics

Tomohide R. Sato,[1] Koji L. Ode,[1] Fukuaki L. Kinoshita,[2,3] and Hiroki R. Ueda[1,3,4,5,*]

[1]Department of Systems Pharmacology, Graduate School of Medicine, The University of Tokyo, Hongo 7-3-1, Bunkyo-ku, Tokyo 113-0033, Japan

[2]Department of Neurology, Graduate School of Medicine, Osaka University, 2-2 Yamadaoka, Suita, Osaka 565-0871, Japan

[3]Laboratory for Synthetic Biology, RIKEN Center for Biosystems Dynamics Research, 1-3 Yamadaoka, Suita, Osaka 565-0871, Japan

[4]Department of Systems Biology, Institute of Life Science, Kurume University, 67 Asahimachi, Kurume, Fukuoka 830-0011, Japan

[5]Lead Contact

*Correspondence: uedah-tky@umin.ac.jp

https://doi.org/10.1016/j.isci.2025.111904

SUMMARY

Nonrapid eye movement sleep is characterized by high-amplitude and low-frequency electroencephalography signals. These signals are thought to be produced by the synchronized activity of cortical neurons, demonstrating the alternating bursting (up) and resting (down) states. Here, such an activity is referred to as up-down oscillation (UDO). Previously, we discussed the importance of the Ca^{2+}-dependent hyperpolarization pathway in the generation of UDO by simulating neuronal activity based on the Hodgkin-Huxley-type model. We herein focus on intracellular Na^+ dynamics. The Na^+-centered model indicates that the activation of voltage-gated Na^+ channels leads to intracellular Na^+ accumulation, which in turn activates Na^+-dependent K^+ (KNa) channels or Na^+/K^+ ATPases, resulting in the down state. Activation kinetics of voltage-gated Na^+ channels are important in shaping the UDO firing. Therefore, our model demonstrates that voltage-gated Na^+ and KNa channels or Na^+/K^+ ATPases are candidate pathways for UDO induction.

INTRODUCTION

Electroencephalogram (EEG) is employed to observe the ensemble activity of cortical neurons during the sleep and awake states. Previous studies have shown that a high-amplitude and low-frequency EEG pattern is observed during nonrapid eye movement (NREM) sleep.[1] The EEG activity is a slow-wave activity. When this activity is perceived, a characteristic electrophysiological firing pattern is detected in the cortical neurons, which is composed of two states: a depolarized bursting phase (up state) and a hyperpolarized resting phase (down state).[2,3] The depolarized phase is referred to as the up state, and the hyperpolarized phase as the down state.[4] Hereafter, we call this alternating up-/down-state pattern as up-down oscillation (UDO). Several computational models including the Hindmarsh-Rose model successfully recapitulated UDO.[5–8] In the Hindmarsh-Rose model, in addition to variables denoting the membrane potential and variables denoting fast ionic components, one variable denoting the adaptation component is found to be crucial for producing a cyclic bursting trajectory.[5] Adaption component requires recording firing activity during bursting and utilizing these data to dynamically adjust its behavior, potentially leveraging memristive properties for adaptive functionality. Memristive properties can be embodied by memristive ion channels[9] or other mem-elements such as memcapacitors.[10] However, molecular entities of these memristive components supporting UDO remain elusive. In a previous study, UDO was achieved using the averaged-neuron (AN) model.[11] This model describes neuronal firing based on the Hodgkin-Huxley model[12] and incorporates 13 components, including receptors of neurotransmitters, ion channels, and Ca^{2+} pumps. The AN model leveraged the concept of mean-field approximation and enabled detailed analyses of individual components. In a later study, a simplified version of the AN model (SAN model)[13] was developed to conduct a mathematical analysis on the mechanisms underlying UDO. In the AN/SAN models, Ca^{2+}-dependent hyperpolarizing currents mediated by Ca^{2+}-dependent K^+ (KCa) channels mainly contribute to the induction of the down state. Meanwhile, the role of Na^+-dependent K^+ (KNa) channels is indicated in a previous study.[14] KNa channels are supposed to regulate the resting membrane potential and the firing rate adaptation.[15,16] The activation of KNa channels is dependent on the intracellular Na^+ concentration. Typically, the increase in the intracellular Na^+ concentration is mediated by voltage-gated Na^+ channels. However, whether the activation of voltage-gated Na^+ channels induces hyperpolarization of the down state in UDO remains unclear. This is because voltage-gated Na^+ channels that activate KNa channels also create depolarizing currents.

Typical voltage-gated Na^+ channels are fully inactivated within a few milliseconds; however, residual Na^+ currents are observed,

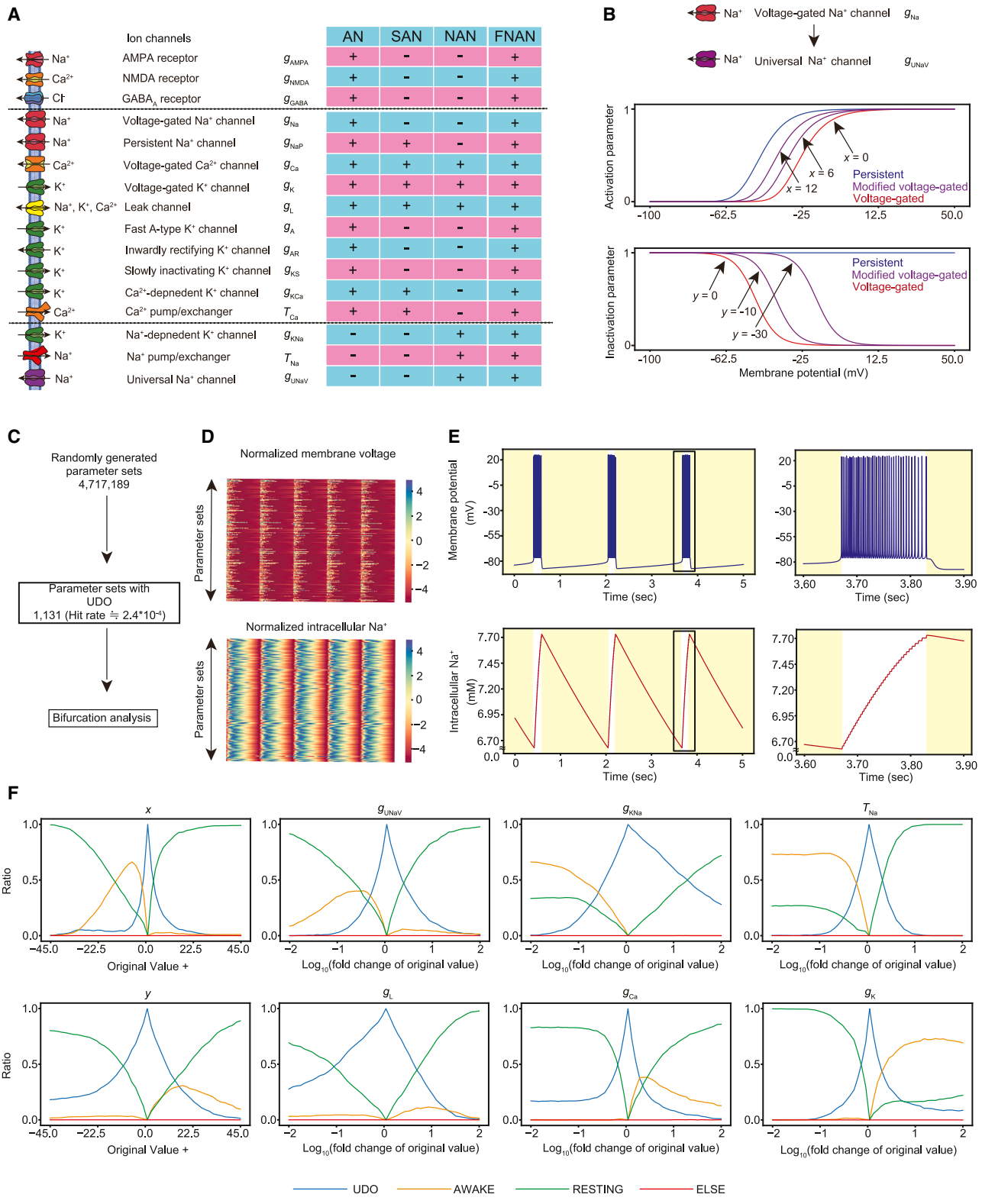

Figure 1. Construction of the NAN model by incorporating UNaV channels

(A) Schematic diagram of the AN, SAN, NAN, and FNAN models. Some of the channels and pumps included in the AN model[11] are included in the other models. In the NAN and FNAN models, KNa channels, UNaV channels, and Na^+ pumps/exchangers are newly incorporated.

(legend continued on next page)

which are referred to as persistent Na^+ currents.[17] An electrophysiological measurement showed that persistent Na^+ currents are observed due to the activation of Na^+ channels at a lower voltage and the slower inactivation of these channels than that of the channels described in the Hodgkin-Huxley model.[18]

Meanwhile, the major factor responsible for Na^+ efflux is Na^+/K^+ ATPases. These ATPases exchange intracellular three Na^+ and extracellular K^+ by consuming the energy of the ATP hydrolysis.[19] This activity is enhanced if the intracellular Na^+ is elevated.[20] Generally, Na^+/K^+ ATPases restore the concentration gradient of Na^+ and K^+ between the inside and outside of the cells, which is counteracted by passive diffusion during the occurrence of the action potential.

The Na^+- and Ca^{2+}-dependent hyperpolarization pathways can similarly work in the up-to-down-state transition. However, such dependencies with different influx and efflux currents as well as baseline concentrations of intracellular Na^+ and Ca^{2+} may lead to different UDO characteristics. Alternatively, these hyperpolarization pathways may serve redundantly for the induction of the down state, leading to the robust induction of UDO. In this study, we investigated the possible role of the Na^+-dependent hyperpolarization pathway in inducing UDO. Furthermore, we modified the previous AN and SAN models to incorporate the changes in the kinetics of the voltage-gated Na^+ channel. We also focused on the quantitative difference between the Na^+- and Ca^{2+}-dependent hyperpolarization pathways. Our results indicated that the former pathway is one of the candidate mechanisms that induce the down state of UDO.

RESULTS

Construction of the NAN model by incorporating the universal voltage-gated Na^+ channel

Tatsuki et al. (2016) demonstrated that the Ca^{2+}-dependent hyperpolarization pathway contributes to the induction of UDO with the AN model.[11] In this model, there is a gradual intracellular Ca^{2+} accumulation during the up state, and such an accumulation activates KCa channels to induce the up-to-down-state transition. During the down state, intracellular Ca^{2+} gradually diminishes due to the action of Ca^{2+} pumps/exchangers. However, the AN model and the subsequent simplified SAN model[13] do not consider the role of Na^+ dynamics in inducing the up-to-down-state transition. A possible mechanism for the induction of the Na^+-dependent down state is the KNa current activation during the up state to induce hyperpolarization and subsequent decrease in intracellular Na^+ by Na^+ pumps/exchangers. Inward Na^+ currents are mainly mediated by voltage-gated and leak Na^+ channels.

To determine whether such an Na^+-dependent mechanism is the underlying mechanism for inducing UDO, we developed an alternative SAN model, taking into consideration the role of the Na^+ dynamics, referred to as the Na^+-centered AN (NAN) model (Figure 1A). This model leverages the concept of mean-field approximation for a population of neurons to extract characteristic dynamics independently of specific neural circuits. The Na^+ dynamics was implemented by voltage-gated Na^+ channels, leak Na^+ channels, and Na^+ pumps/exchangers. Furthermore, we considered the role of KNa channels (Figure 1A).

Persistent Na^+ currents are incorporated in the AN and SAN models[11,13]; Figure 1B illustrates the inactivation and activation curves of persistent Na^+ currents. As regards the Na^+ current, we herein consider voltage-gated Na^+ channels, which are expressed as follows:

$$I_{NaV} = g_{NaV} m_{NaV}^3 h_{NaV} (V - V_{Na}) \quad \text{(Equation 1)}$$

$$m_{NaV} = \alpha_m / (\alpha_m + \beta_m) \quad \text{(Equation 2)}$$

$$\alpha_m = 0.1(V + 33 + x) / [1 - exp(-(V + 33 + x) / 10] \quad \text{(Equation 3)}$$

$$\beta_m = 4\, exp(-(V + 53.7 + x) / 12) \quad \text{(Equation 4)}$$

$$\frac{dh_{NaV}}{dt} = 4\,(\alpha_h\,(1 - h_{NaV}) - \beta_h\, h_{NaV}) \quad \text{(Equation 5)}$$

$$\alpha_h = 0.07\, exp\,(-(V + 50 + y) / 10) \quad \text{(Equation 6)}$$

$$\beta_h = 1/[1 + exp\,(-(V + 20 + y) / 10)] \quad \text{(Equation 7)}$$

where g_{NaV} denotes the conductance of voltage-gated Na^+ channels; m_{NaV}, activation parameter of voltage-gated Na^+ channels; h_{NaV}, inactivation parameter of voltage-gated Na^+ channels; V_{Na}, reversal potential of voltage-gated Na^+ channels; V, membrane voltage; and t, time.

(B) The changes in the activation/inactivation curve of UNaV channels alter the persistency of UNaV currents. (Left) The blue curve denotes the activation curve of persistent Na^+ channels, whereas the purple curves denote the activation curve of modified voltage-gated Na^+ channels (universal Na^+ channels). The red curve in the left figure denotes the activation curve of voltage-gated Na^+ channels with typical voltage sensitivity. When the value of parameter *x* increases, the purple curve shifts leftward (i.e., increased persistency). (Right) The blue, purple, and red curves denote the inactivation curve of the corresponding channels, as shown in the left panel. When the value of parameter *y* decreases, the purple curve shifts rightward (i.e., increased persistency). The mathematical formulas for these channels are taken from the study by Tatsuki et al. (2016),[11] which is based on the study by Compte et al. (2003).[14]

(C) Workflow of the random parameter search. A total of 1,131 parameter sets of the NAN model with UDO were obtained. The UDO parameter sets were subsequently used in the bifurcation analysis.

(D) The normalized membrane potential and intracellular Na^+ are presented for all the 1,131 UDO parameter sets.

(E) Representative UDO and intracellular Na^+ concentration of the NAN model. The right panels are magnified images.

(F) Results of the bifurcation analysis with all parameters in the NAN model. Each panel explains the result of the bifurcation analysis for the indicated parameter. Each channel conductance or time constant was gradually changed within the range from 10^{-2} to 10^2 times its original value. The parameters *x* and *y* were changed within the range from −45.0 to +45.0 from the original value. The vertical axis shows the ratio of the parameter sets showing the indicated firing pattern (UDO, AWAKE, RESTING, or other patterns). The criteria for the classification are based on the previous study[11] (see STAR Methods). See also Figures S1, S2, S7, and Table S1.

In these equations, the activation parameter m_{NaV} denotes the voltage sensitivity for the channels' activation. The inactivation parameter h_{NaV} denotes the voltage sensitivity for the channels' inactivation. These voltage sensitivities (i.e., m_{NaV} and/or h_{NaV}) can be dynamically modulated through posttranslational modifications. Thompson et al. (2017) reported that sodium channel protein type 2 subunit alpha 1 (SCN2a1) phosphorylation by calcium/calmodulin-dependent protein kinase II (CaMKII) resulted in the rightward shift of the inactivation curve.[21] In addition, Daskal and Lotan reported that the phosphorylation of rat brain Na^+ channels by protein kinase C resulted in the rightward shift of the activation curve.[22] Inactivation failure can lead to Na^+ currents with some degree of persistency against voltage dynamics (herein referred to as "persistent-like" Na^+ currents). In our model scheme, these "persistent-like" Na^+ currents can be described by either increasing the parameter x or decreasing the parameter y in Equations 3, 4, 5, 6, and 7. An increase in x leads to the upregulation of currents mediated by the channels as x represents the shift of the activation curve and the leftward shift activates the channels at a lower membrane voltage. Contrarily, a decrease in y leads to the upregulation of currents mediated by the channels (Figure 1B) as y represents the shift of the inactivation curve and the rightward shift causes the channels to remain active at a higher membrane voltage. Thus, either increasing x or decreasing y leads to the channels' activity similar to that of persistent Na^+ channels (Figure 1B). If $x = y = 0$, the equations represent voltage-gated Na^+ channels without such voltage-sensitivity modifications and are utilized in the AN and other models.[11,13] To distinguish this "normal" setting for voltage-gated Na^+ channels, we will call voltage-gated Na^+ channels with parameters x and y (i.e., $x \neq 0$ and $y \neq 0$) universal voltage-gated Na^+ (UNaV) channels.

The dependence of the activation parameter of KNa channels on intracellular Na^+ concentration was mimicked by fitting previously reported data.[16] However, the KCa channels and Ca^{2+} pumps/exchangers involved in the SAN model were not considered in the NAN model, assuming that the roles of KCa currents can be replaced by those of KNa currents. The other receptors and channels found in the SAN model were incorporated in the NAN model as they are essential in the induction of a bursting pattern and the AWAKE-UDO transition[13] (Figure 1A). Na^+ pumps/exchangers were introduced as linearized pumps, in which the speed of Na^+ uptake follows the sodium current and intracellular Na^+ concentration. Briefly, the differences between the SAN and NAN models are the presence of UNaV channels, KNa channels, and Na^+ pumps/exchangers and the absence of KCa, persistent Na^+ channels, and Ca^{2+} pumps/exchangers.

To find parameter sets that induce UDO with the NAN model, we comprehensively searched for parameters describing the conductance of ion channels, time constant for Na^+ efflux, and parameters x and y for UNaV channels (Figure 1C). Of the 4,000,000 randomly generated parameter sets, 2.4×10^{-4}% (~1,000) demonstrated UDO, indicating that the pivotal roles of KCa currents in the induction of UDO can be replaced by those of KNa currents. UDO demonstrated intracellular Na^+ waves that were coupled with the membrane potential (Figures 1D and 1E). Notably, the representative parameter set was selected by conducting principal-component analysis (PCA) to the ~1,000 parameter sets with UDO. The typical parameter set was selected from the area with parameter set enrichment.

To explore the potential roles of each parameter in UDO induction, we conducted bifurcation analysis, where each channel conductance or time constant was gradually changed within the range of 10^{-2} to 10^2 times its value. The parameters x and y were changed within the range of −45.0 to +45.0 from the original value (Figure 1F).

Figures 1F and S1A present the bifurcation diagrams for each parameter in the NAN model. An increase in x led to the AWAKE-UDO transition (see the yellow and cyan curves). This is consistent with the anticipated role of the Na^+-dependent hyperpolarization pathway in inducing the down state. An increase in x leads to an effective Na^+ accumulation at a lower membrane voltage, which can activate KNa channels to induce hyperpolarization for the down state. Similarly, an increase in Na^+ accumulation by a lower y or a higher UNaV channel (g_{UNaV}) conductance leads to the AWAKE-UDO transition, further supporting the role of the Na^+-dependent hyperpolarization pathway in inducing the down state. Interestingly, parameter x may have a strict constraint for UDO induction. This is evident from the narrow range of UDO (cyan curve) shown in the x bifurcation diagram compared with those in y and g_{UNaV} (Figure 1F). The strict constraint for parameter x is also evident from the distribution of the parameters inducing UDO (Figure S1B). Furthermore, the distribution indicates that the value of x should be strictly positive, suggesting that a lower voltage threshold for the activation curve of UNaV channels is necessary for UDO induction in the NAN model. However, the distribution of parameter y indicates the mild constraint of this parameter for UDO induction (Figure S1B).

The importance of intracellular Na^+ level for the induction of the down state in the NAN model is also supported by the finding that an increase in the conductance of the KNa channels (g_{KNa}) and the time constant of Na^+ pumps/exchangers (τ_{Na}) resulted in the AWAKE-UDO transition (see yellow and cyan curves). This is consistent with the anticipated role of the Na^+-dependent hyperpolarization pathway driven by g_{KNa}. An increase in τ_{Na} is expected to promote effective accumulation of intracellular Na^+. Interestingly, g_{KNa} may have a loose constraint for UDO induction.

Meanwhile, an increase in the conductance of voltage-gated Ca^{2+} (g_{Ca}) or voltage-gated K^+ (g_K) channels led to the UDO-AWAKE transition. The NAN model does not involve the KCa channels, and, thus, the main role of voltage-gated Ca^{2+} channels in the NAN model may be to upregulate neuronal excitability. The roles of voltage-gated K^+ channels in inducing the AWAKE firing pattern can be estimated through an in-depth investigation of the intracellular Na^+ level: at a higher g_K, the intracellular Na^+ does not accumulate even in the up state, indicating the attenuation of Na^+ influx (Figure S1C).

Notably, the changes in the conductance of the leak channels (g_L) had less effect on the UDO-AWAKE transition, indicating that leak channels are not important in the induction of UDO in the NAN model.

The NAN model does not include ion channels depending on the intracellular Ca^{2+} (e.g., KCa channels). However, we kept the voltage-gated Ca^{2+} channels in the NAN model due to the

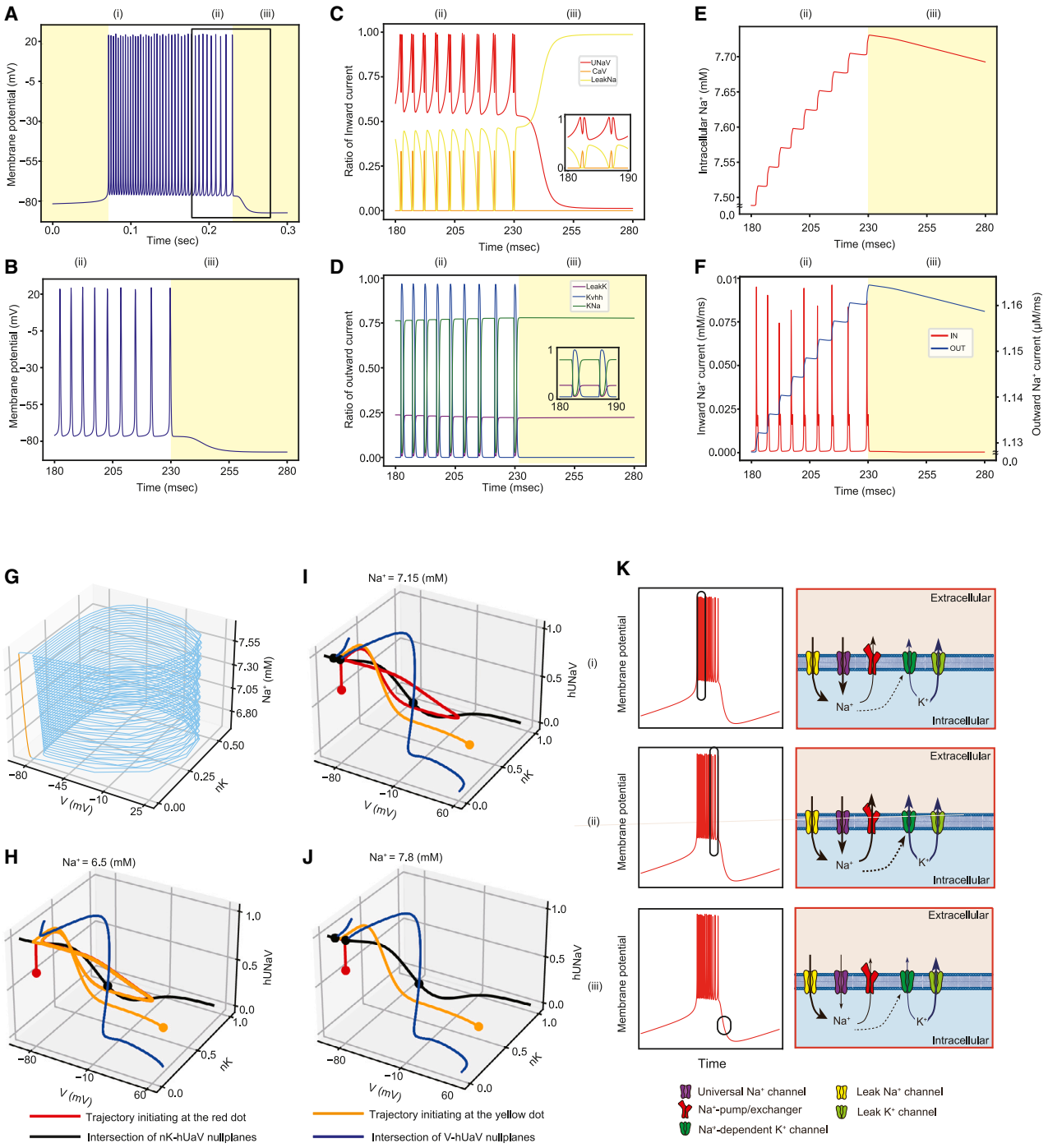

Figure 2. Accumulation of Na^+ drives the up-to-down-state transition

(A and B) Representative time course of membrane voltage in the NAN model. The parameter set for this graph is the same as that for Figure 1E. The yellow areas denote the down state, whereas the white areas denote the up state. The area surrounded by the black square indicates the place where it is magnified in panels. (B) is the magnified image of (A).

(C–F) The time in Figures 2C–2F is the same as that in Figure 2B. (C) Time course of inward currents. "UNaV" denotes currents with UNaV channels; "CaV," currents with voltage-gated Ca^{2+} channels; and "LeakNa," currents with leak Na^+ channels. The bottom-right figure is the magnification of the time courses of these currents. (D) Time course of outward currents. "LeakK" denotes the currents with leak K^+ channels; "Kvhh," currents with voltage-gated K^+ channels; and "KNa," currents with KNa channels. The bottom-right figure is the further magnification of the time courses of these currents. (E) Time course of intracellular Na^+. (F) Time course of the inward/outward Na^+ currents.

(legend continued on next page)

following reasons. We tested different versions of the NAN model without voltage-gated Ca^{2+} channels (NAN model with $g_{Ca} = 0$, Figure S2A). This model is capable of inducing UDO. The distribution also indicates that the value of x should be strictly positive, suggesting that a lower voltage threshold for the activation curve of UNaV channels is necessary to induce UDO in this model (Figure S2B). However, the bifurcation diagram of the conductance of UNaV channels (g_{UNaV}) shows that either an increase or a decrease in the conductance can lead to the UDO-AWAKE transition (compare g_{UNaV} panel in Figures S2C and 1F). Briefly, the role of UNaV channels in inducing UDO is unclear. This is probably because Na^+ currents have two roles: a facilitator of depolarization and a facilitator of hyperpolarization induced by the KNa currents. Meanwhile, the voltage-gated Ca^{2+} channels in the NAN model only play the role of a facilitator of depolarization. Thus, the presence of voltage-gated Ca^{2+} channels (i.e., original NAN model in Figure 1A) may support the role of UNaV channels as a facilitator of hyperpolarization by activating the KNa currents. The clear distinction of the UDO-AWAKE transition in the g_{UNaV} bifurcation was demonstrated in the original NAN model.

Na^+ accumulation drives the up-to-down-state transition

We investigated the mechanism of UDO by analyzing the ordinary differential equations (ODEs) trajectory around the up-to-down-state transition (Figures 2A and 2B). Figures 2C and 2D illustrate that the action potential during the up state is initiated by UNaV channels and sustained by voltage-gated Ca^{2+} channels. The action potential is inhibited by the activation of voltage-gated K^+ and KNa channels. During the down state, most of the hyperpolarization currents are mediated by the KNa current. This is contrary to what is observed in the AN and SAN models, demonstrating the importance of KCa currents in the hyperpolarization during the down state. In the NAN model, leak K currents also constitute the hyperpolarization current, which is consistent with the SAN model. Figures 2E and 2F illustrate that intracellular Na^+ cumulatively rises during the depolarization phase (i.e., the up state) and then continuously decreases after the onset of the down phase. The increase and decrease in the intracellular Na^+ concentration can be explained by the altered ratio of the overall activity between the UNaV/Leak Na^+ channels (IN) and the Na^+ pumps (OUT) (Figure 2F).

To analyze the mechanism behind the down-state induction, we plotted the trajectory of UDO in the phase space (Figure 2G). The NAN model has four variables in the ODEs, namely, V, membrane potential; nK, dimensionless quantity associated with the activation of voltage-gated K^+ channels; hUNaV, dimensionless quantity associated with the inactivation of UNaV channels; and Na^+, intracellular Na^+ concentration. The coiled (blue trajectory) and straight (yellow trajectory) parts correspond to the up and down states, respectively. Figures 2H–2J present the intersection of nullplanes at fixed Na^+ concentrations. As the nullplane is a set of points where the first derivative of a certain direction is zero, a system on the intersection of two nullplanes only evolves to the remaining variable; for example, on the intersection of V-nK null planes, only the hUNaV variable evolves. Thus, null plane analysis enables us to understand the approximate ODE dynamics.

At a low Na^+ concentration (6.5 mM), the trajectory converges to the stable limit cycle (Figure 2H), which corresponds to the up state of UDO. At a moderate Na^+ concentration (7.15 mM), at least two stable states are observed, a stable point and a stable limit cycle, which correspond to the down and up states, respectively (Figure 2I). At a high Na^+ concentration (7.8 mM), the stable limit cycle does not exist, and the trajectory converges to the stable point corresponding to the down state (Figure 2J). Figure 2K summarizes the proposed mechanism of down-state induction by the Na^+-dependent hyperpolarization pathway. During the early phase of the up state (i), voltage-gated Na^+ channels and leak Na^+ channels are opened, and Na^+ enters the intracellular environment. At this stage, the accumulation of intracellular Na^+ is insufficient to activate KNa channels. During the late stage of the up state, the intracellular Na^+ is gradually accumulated (ii), and, when it reaches a sufficiently high level, the power of KNa currents is strong enough to induce the down state through the activation of KNa channels (iii). Concisely, the phase planes of the NAN model show that the alteration between the up and down states is associated with the Na^+ concentration-dependent transition of stable states (Figure 2K).

Parameter x is important for controlling several features of wave pattern in the NAN model

Next, we investigated how several features of the wave patterns produced in the NAN model are regulated by each parameter. Each UDO parameter found in the random parameter search (Figure 1C) slightly decreased or increased, and the effect of the slight change on UDO was quantified. For the UDO characterization, we focused on the up- and down-state duration, oscillation period (defined as the duration of the up and down states), amplitude of intracellular Na^+ oscillation, and interspike interval (ISI) during the up state. Figures 3A–3G demonstrate that parameter x extended the down-state duration, oscillation period, and Na^+ oscillation amplitude and shortened the ISI. This suggests

(G) Trajectory of the NAN model plotted on a three-variable space: membrane voltage (V), activation parameter of the voltage-gated K^+ channel (nK), and intracellular Na^+. The blue line denotes the trajectory corresponding to the up state, whereas the orange line denotes the trajectory corresponding to the down state.

(H–J) The intersection of V nullplane and inactivation parameter of the universal Na^+ channel (hUNaV) nullplane is denoted by the blue curve, whereas the intersection of nK nullplane and hUNaV nullplane is denoted by the black curve. The red or yellow dot denotes the initial condition of the integration with ODEs. The black dots denote the fixed point(s) of the system. To reduce the number of variables from four to three, Na^+ is fixed at indicated values (6.5 mM, H; 7.15 mM, I; or 7.8 mM, J).

(K) Schematic representation of the mechanisms inducing UDO with the Na^+-dependent hyperpolarization pathway. (i) During the up state, there are transient Na^+ inward currents, and Na^+ is pumped out by Na^+ pumps. (ii) Gradually, intracellular Na^+ accumulates and the up state is terminated due to the dominance of KNa currents. (iii) During the down state, intracellular K^+ exits the cell mainly through KNa channels. Note that (i)–(iii) shown in Figures 2A–2F correspond to schemes (i)–(iii).

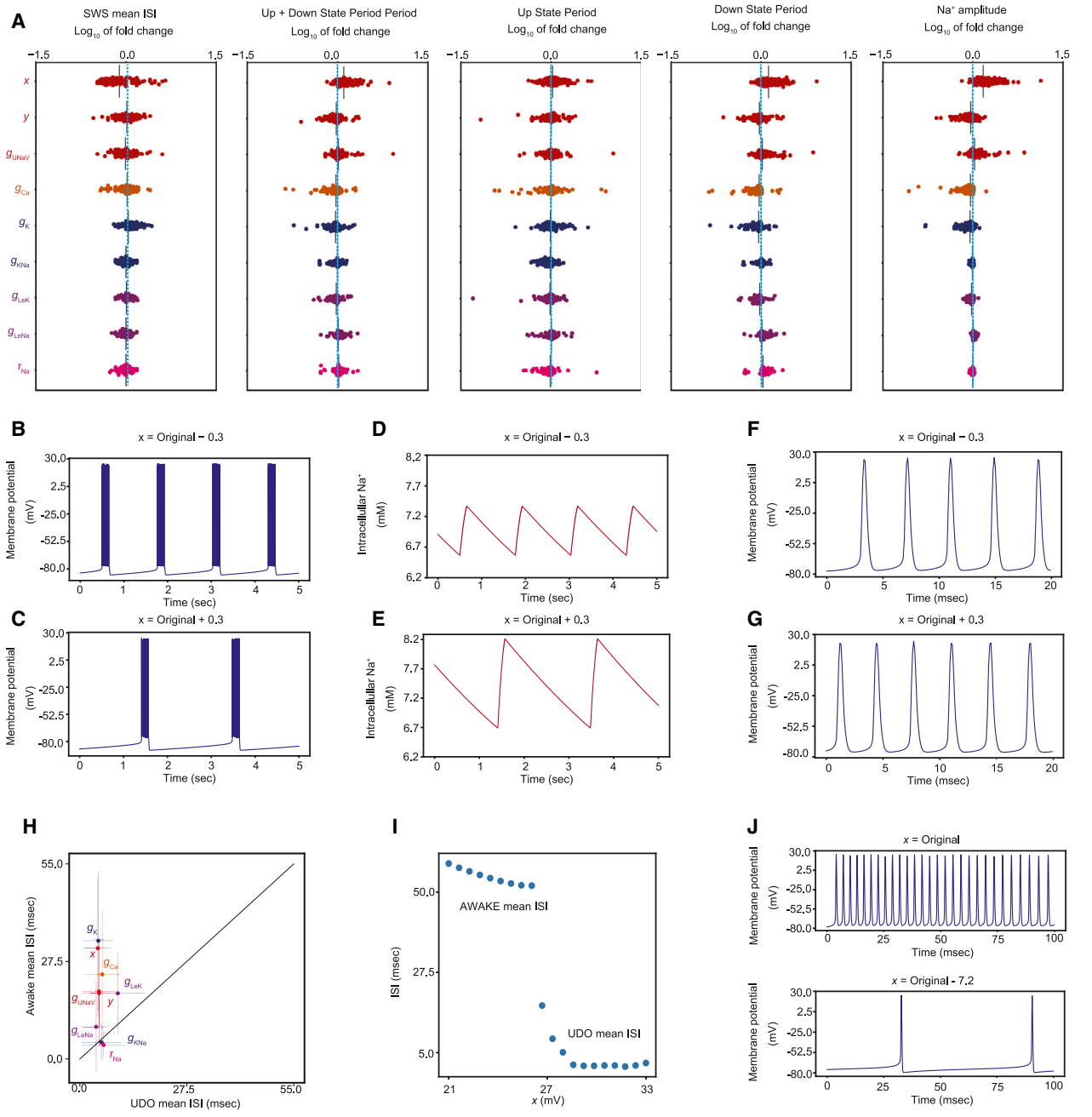

Figure 3. The activation parameter of UNaV is important for controlling several features of the wave pattern in the NAN model

(A) The effect of the slight upregulation of the value of each parameter alters the UDO characteristics. All the parameter sets inducing UDO are used in the analysis. For parameters x and y, the UDO characteristics are calculated when the value of x and y is (1) 0.5 lower and (2) 0.5 higher than the original value. For the other parameters, the UDO characteristics are calculated when the value is (1) 0.975 times of the original value and (2) 1.025 times of the original value. The value calculated in (2) is divided by the value calculated in (1). The blue dotted line shows Log_{10} of fold change = 0 (i.e., perturbation does not alter each UDO characteristic).

(B and C) Representative trace of the firing pattern when the value of x is (B) 0.5 lower and (C) 0.5 higher than the original value.

(D and E) Representative trace of the intracellular Na^+ oscillation when the value of x is (D) 0.5 lower and (E) 0.5 higher than the original value.

(F and G) Representative trace showing the ISI when the value of x is (F) 0.5 lower and (G) 0.5 higher than the original value.

(H) The trends of the ISI in UDO and AWAKE firing patterns. To effectively induce the AWAKE firing pattern for the majority of parameter sets with UDO, the amount of perturbation was chosen based on the bifurcation analysis in Figure 1F (x, −7.2; y, +16.2; g_K, $\times 10^{1.52}$; g_{Ca}, $\times 10^{0.4}$; g_{LeK}, $\times 10^{-2.0}$; g_{LeNa}, $\times 10^{0.88}$; g_{UNaV}, $\times 10^{-0.48}$; g_{KNa}, $\times 10^{-2.0}$; τ_{Na}, $\times 10^{-0.96}$). The parameter sets, which show the AWAKE firing pattern when each parameter is changed as above, are selected for each

(legend continued on next page)

that x plays a major role in inducing UDO and Na^+ dynamics in this model.

It has been demonstrated that the ISI during the up state of UDO tends to be smaller than that during the wake time.[2,23] A similar trend can be observed when bifurcation from UDO to AWAKE was induced by changing the parameters x, y, g_K, g_{Ca}, and g_{UNaV}. However, such a reduced ISI in the up state was hardly observed when bifurcation was induced by changing g_{KNa} and τ_{Na} (Figures 3H–3J). Parameters x, y, g_K, g_{Ca}, and g_{UNaV}, but not g_{KNa} and τ_{Na}, are all related to the ion channels whose activation is directly regulated by membrane potential. This result indicates that the bifurcation of UDO to the AWAKE firing pattern in *in vivo* neurons is associated with the changes in voltage-related channel regulation.

To summarize, the increase in parameter x, which indicates the shift in the activation curve of voltage-gated Na^+ channels to make the Na^+ currents more persistent, leads to the elongation of the down-state duration and Na^+ oscillation amplitude as well as shortening of the mean ISI of the up state in UDO.

The Na^+-dependent hyperpolarization pathway can also be implemented by Na^+/K^+ ATPase

In the NAN model, Na^+ pumps/exchangers are described by Na^+ pumps with linear kinetics. In the actual neurons, however, majority of the Na^+ efflux is mediated by Na^+/K^+ ATPases that exchange 2 K^+ and 3 Na^+ ions coupled with ATP hydrolysis.[24] To explore the possible contribution of Na^+/K^+ ATPases as a molecular nature for the export of Na^+ from the neurons, we developed an alternative model (Figure 4A). We speculated that hyperpolarization driven by Na^+/K^+ ATPases is the main source of hyperpolarization currents inducing the down state. To focus on such a role for Na^+/K^+ ATPases, the revised model with Na^+/K^+ ATPases does not include KNa channels, which support the induction of the down state in the NAN model, as previously described. Among the 50,000,000 randomly generated parameter sets, 2.0×10^{-5}% (~1,000) of them achieved UDO in the revised NAN model, suggesting that the pivotal roles of KNa currents in inducing the UDO can be replaced by Na^+/K^+ ATPase currents. The intracellular Na^+ concentration oscillates with the membrane potential (Figures 4B and 4C). Figures 4D and S4A present the bifurcation diagram in the revised NAN model. The decrease in the conductance of Na^+/K^+ ATPases (g_{NaK}) resulted in the UDO-AWAKE transition, supporting the importance of Na^+/K^+ ATPases-mediated hyperpolarization currents for the induction of the down state. Figures 4E and S4B illustrate the distribution of each parameter. The distribution of g_{NaK} observed in the UDO parameter sets is restricted in the larger g_{NaK} (Figure 4E), suggesting that a sufficiently large g_{NaK} is required to induce UDO.

Figures 4F–4I illustrate that the action potential during the up state is initiated by UNaV channels. Such an action potential is ceased by the activation of voltage-gated K^+ channels and Na^+/K^+ ATPases. During the down state, ~75% of the hyperpolarization current is mediated by Na^+/K^+ ATPases currents. The rest of the ~25% hyperpolarization current is mediated by leak K^+ currents, consistent with the SAN model.[13] Figures 4J and 4K illustrate that intracellular Na^+ cumulatively increases during the depolarization phase (i.e., the up state) and then continuously decreases after the onset of the down state. The increase and decrease in intracellular Na^+ concentration can be explained by the altered ratio of the overall activity between UNaV/Leak Na channels(IN) and Na^+/K^+ ATPases (OUT) (Figure 4K).

The role of parameter x in inducing UDO is consistent between the NAN and the revised NAN models: increase in parameter x elongated down-state duration and Na^+ oscillation amplitude and decreased ISI in the up state during UDO (Figures 4L–4O and S4C). Similar to the case of g_{NaK}, the perturbation on g_{NaK} resulted in the decrease in the ISI across the UDO-AWAKE transition state, which is opposite direction observed in the tendency of ISI transition *in vivo*, suggesting that other factors, such as x, are responsible for the UDO-AWAKE transition *in vivo*.

The Full-NAN model shows the importance of the Na^+-dependent hyperpolarization pathway

To evaluate the role of the Na^+-dependent hyperpolarization pathway in the presence of multiple pathways, some of which are not explicitly described in the NAN and SAN models, we developed a full-NAN (FNAN) model. The FNAN model includes all channels/pumps in the original AN model[11] as well as the NAN model. This model consists of 3 neurotransmitter receptors and 13 ion channels and pumps (see Figure 1A). Among the ~24,000,000 randomly generated parameter sets, 8.9×10^{-5}% (~2,000) of them achieved UDO. To identify which ion channels/pumps play a pivotal role in the induction of UDO, we next conducted "knockout experiments" where we removed the contribution of each ion channel/pump. The removal of gamma-aminobutyric acid receptor (GABAR) currents did not disrupt UDO in majority of the parameter sets (Figure S5A). Thus, we decided to exclude GABAR in the subsequent analysis. The knockout of KNa channels led to the UDO-AWAKE transition in majority of the parameter sets, which otherwise induced UDO. Meanwhile, the knockout of KCa channels did not alter the firing pattern in most cases (Figure 5A), suggesting that, in majority of the parameter sets in the FNAN model, the Na^+-dependent hyperpolarization (driven by KNa channels) is more dominant than the Ca^{2+}-dependent hyperpolarization (driven by KCa channels) in inducing the down state. Indeed, only a few parameter sets exhibited an AWAKE firing pattern when the conductance of KCa channels was set to zero; moreover, among these 40 parameter sets, 31 showed an AWAKE firing pattern by the knockout of KNa channels (Figure S5B). In other words, KCa channels are only fully responsible for the induction of UDO for only the remaining 9 out of 1,444 parameter sets. The prominent role of KNa

parameter's analysis. The mean and standard deviation of ISI of the firing pattern are calculated for each parameter set. Dots with color denote the average of the mean ISI of the parameter sets, and bars with color denote the standard deviation of the mean ISI of the parameter sets.

(I) Representative change of the mean ISI when the value of parameter x gradually changes in the representative parameter set.

(J) Representative trace showing the ISI when the firing patterns are UDO (upper) and AWAKE (lower). The UDO-AWAKE transition is induced by lowering the value of parameter x. See also Figure S3.

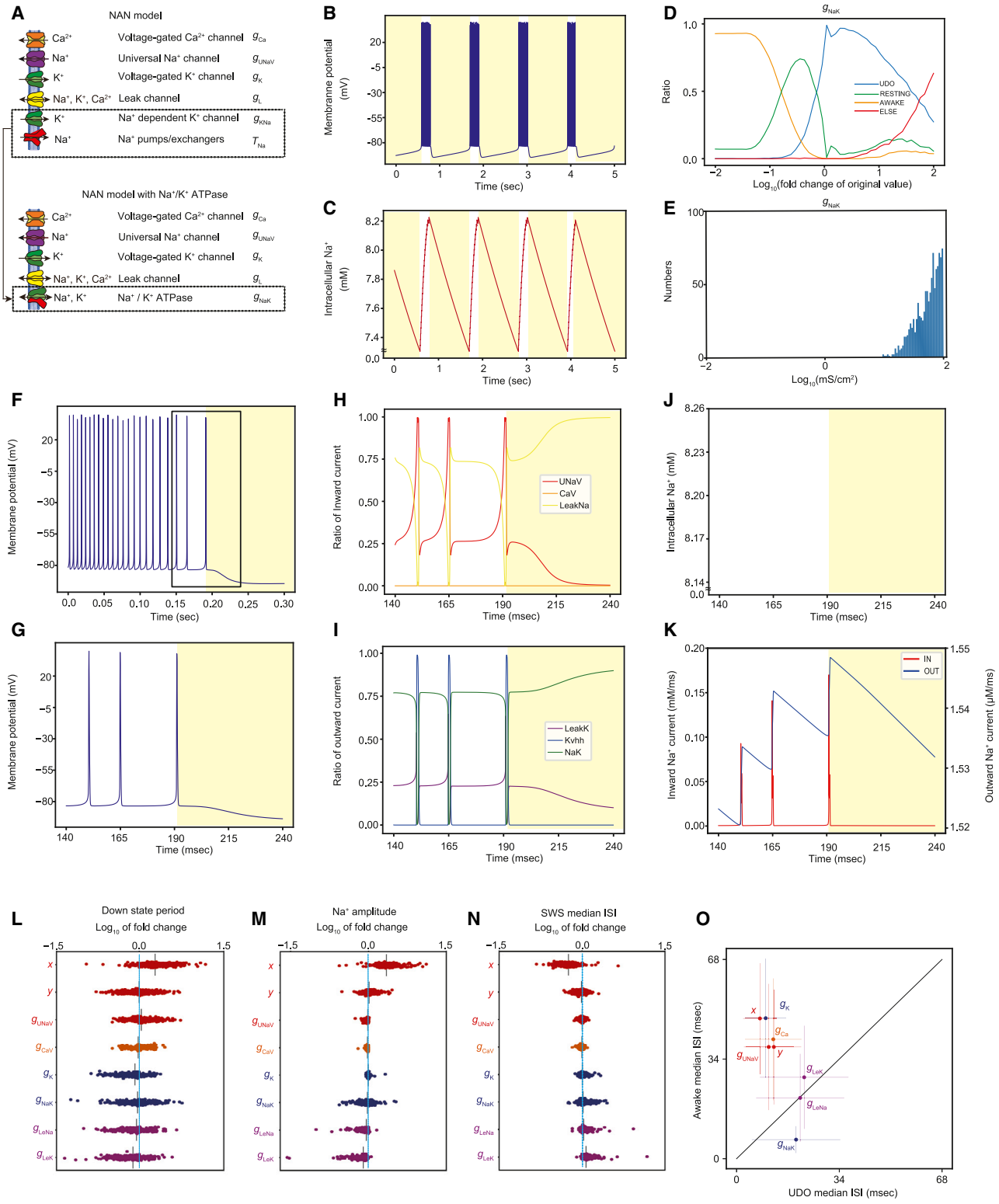

Figure 4. The Na^+-dependent hyperpolarization pathway can also be implemented by the Na^+/K^+ ATPase

(A) Schematic diagram of the NAN model with Na^+/K^+ ATPases.

(B and C) Representative UDO and intracellular Na^+ concentration of the NAN model with Na^+/K^+ ATPases.

(legend continued on next page)

channels or the Na^+-dependent hyperpolarization pathway is further supported by the representative trace of the FNAN model. Figure S5C illustrates that the peak and trough of the Na^+ dynamics are correlated with the beginning and ending of the down state, whereas those of the Ca^{2+} dynamics do not show a consistent increase or decrease during the up or down state, respectively.

The role of UNaV channels, particularly for parameter x, is mostly conserved in the FNAN and NAN models. Similar to the case of the NAN model, the ISI shortening in the up state of UDO was observed when AWAKE was induced by changing parameters x, y, and g_{UNaV} (Figure 5B). Such a trend was hardly observed when the bifurcation was induced by changing g_{KNa} and τ_{Na} in the FNAN model, also consistent with the case of the NAN model.

Furthermore, the FNAN model obscures the consistent change in wave features (i.e., down-state period, Na^+ amplitude, and ISI in the up state) upon the increase/decrease in parameter x (Figure S5D; see also Figure 3A). This is possibly because the FNAN model includes the redundant sources of inward Na^+ currents, such as voltage-gated and persistent Na^+ channels.

To determine whether the role of the Na^+-dependent hyperpolarization pathway revealed so far requires the assumption in the mean-field approximation of the model, we developed a neuronal network with the FNAN model, in which neurons are explicitly connected with N-methyl-D-aspartate (NMDA)- and alpfa-amino-3-hydroxy-5-methyl-4-isoxazolepropionic acid (AMPA)-mediated synaptic connections without the mean-field approximation (Figure 5C). Note that we set g_{GABA} to 0 because UDO persists without GABAergic currents.[2] We simulated the behavior of the network FNAN model with 100 representative parameter sets. Figure 5D shows the representative behavior of the network model exhibiting UDO and AWAKE firing pattern. Subsequently, we determined whether the tendency of ISI observed in the FNAN/NAN models is also preserved in this network model (Figure S6A). The perturbations to each parameter are given so that the wave pattern changes from UDO to AWAKE. The amount of perturbation is determined based on the bifurcation diagram of each parameter (Figure S6B). Similar to the case of the single-cell FNAN model (Figure 5B), ISI shortening in the up state of UDO was observed when AWAKE was induced by changing parameters x, y, and g_{UNaV} (Figure 5E). Such a trend was hardly observed when the bifurcation was induced by changing g_{KNa} in the network FNAN model, which is consistent with the case of the single-cell FNAN model.

In summary, at least part of the role of the Na^+-dependent hyperpolarization pathway in the NAN model is conserved in the FNAN model regardless of the assumption of mean-field approximation.

DISCUSSION

Possible mechanism for UDO with the NAN model

In this study, we developed the NAN model, which induces the down state through the activation of K^+ currents triggered by intracellular Na^+. The NAN model showed that the KNa channels, which have been reported to induce hyperpolarization after bursting,[15,25] are capable of driving UDO. UDO is induced through a series of events summarized as follows. (1) During the up state, Na^+ enters mainly through voltage-gated Na^+ channels and leak Na^+ channels to increase the intracellular Na^+ concentration. (2) The up-to-down-state transition occurs when the intracellular Na^+ concentration reaches a certain threshold to activate KNa channels. (3) During the down state, Na^+ exits through Na^+-pump/exchangers to decrease the intracellular Na^+ concentration. In summary, the intracellular Na^+-dependent hyperpolarizing current drives the up-to-down-state transition. Compte et al. (2003) reported the importance of KNa channels by leveraging complex excitatory-inhibitory neuronal networks.[14] Our study demonstrated the significance of KNa channels independent of such intricate connections and the contribution of inhibitory neurons. The Na^+-dependent hyperpolarization pathway could be implemented by several molecules other than the KNa channels. For example, we demonstrated that Na^+/K^+ ATPases create a hyperpolarizing current dependent on the accumulation of the intracellular Na^+ (Figure 4).

In the Na^+-dependent hyperpolarization pathway, the activation of the hyperpolarizing current should be initiated in a neuronal activity-dependent manner. An increase in parameter x of voltage-gated Na^+ channels, which denotes the negative shift of the activation curve, results in the increase in neuronal activity. Therefore, an increase in x leads to UDO (through

(D) Results of the bifurcation analysis with all parameter sets by changing the value of parameter g_{Nak}. The classification criteria of UDO, AWAKE, RESTING, and ELSE follow those of Tatsuki et al. (2016).[11]

(E) The distributions of the value of the conductance of Na^+/K^+ ATPases in all parameter sets inducing UDO in the NAN model with Na^+/K^+ ATPases.

(F and G) Representative time course of the membrane voltage in the NAN model with Na^+/K^+ ATPases. The area surrounded by the black square indicates the place where it is magnified in the subsequent imaging. (G) The magnified image of (F) in the area surrounded by the black square.

(H–K) The time in Figures 4H–4K is the same as that in Figure 4G. (H) Time course of inward currents. "UNaV" denotes the currents with UNaV channels; "CaV," currents with voltage-gated Ca^{2+} channels; and "LeakNa," currents with leak Na^+ channels. (I) Time course of outward currents. "LeakK" denotes the currents with leak K^+ channels; "Kvhh," currents with voltage-gated K^+ channels; and "NaK," currents with Na^+/K^+ ATPases. (J) Time course of intracellular Na^+. (K) Time course of the inward/outward Na^+ currents.

(L–N) The effect of slight upregulation of the value of each parameter alters the UDO characteristics. All the parameter sets inducing UDO are used in the analysis. For parameters x and y, the UDO characteristics are calculated when the value of x and y is (1) 0.5 lower and (2) 0.5 higher than the original value. For the other parameters, the UDO characteristics are calculated when the value is (1) 0.975 times and (2) 1.025 times of the original value. The value calculated in (2) is divided by the value calculated in (1). The blue dotted line shows Log_{10} of fold change = 0 (i.e., perturbation does not alter each UDO characteristic).

(O) Trends of the ISI in the UDO and AWAKE firing pattern. To effectively induce the AWAKE firing pattern for the majority of the parameter sets with UDO, the amount of perturbation was chosen based on the bifurcation analysis in Figures 4D and S4D (x, −3.6; y, +7.0; g_K, $\times 10^{0.48}$; g_{Ca}, $\times 10^{0.32}$; g_{LeK}, $\times 10^{-1.84}$; g_{LeNa}, $\times 10^{0.48}$; g_{UNaV}, $\times 10^{-0.4}$; g_{NaK}, $\times 10^{-1.44}$). The parameter sets showing the AWAKE firing pattern when each parameter is changed as above are selected for each parameter's analysis. The mean and standard deviation of ISI of the firing pattern are calculated for each parameter set. Dots with color denote the average of the mean ISI of the parameter sets, and bars with color denote the standard deviation of the mean ISI of the parameter sets. See also Figures S4, S7, and Table S2.

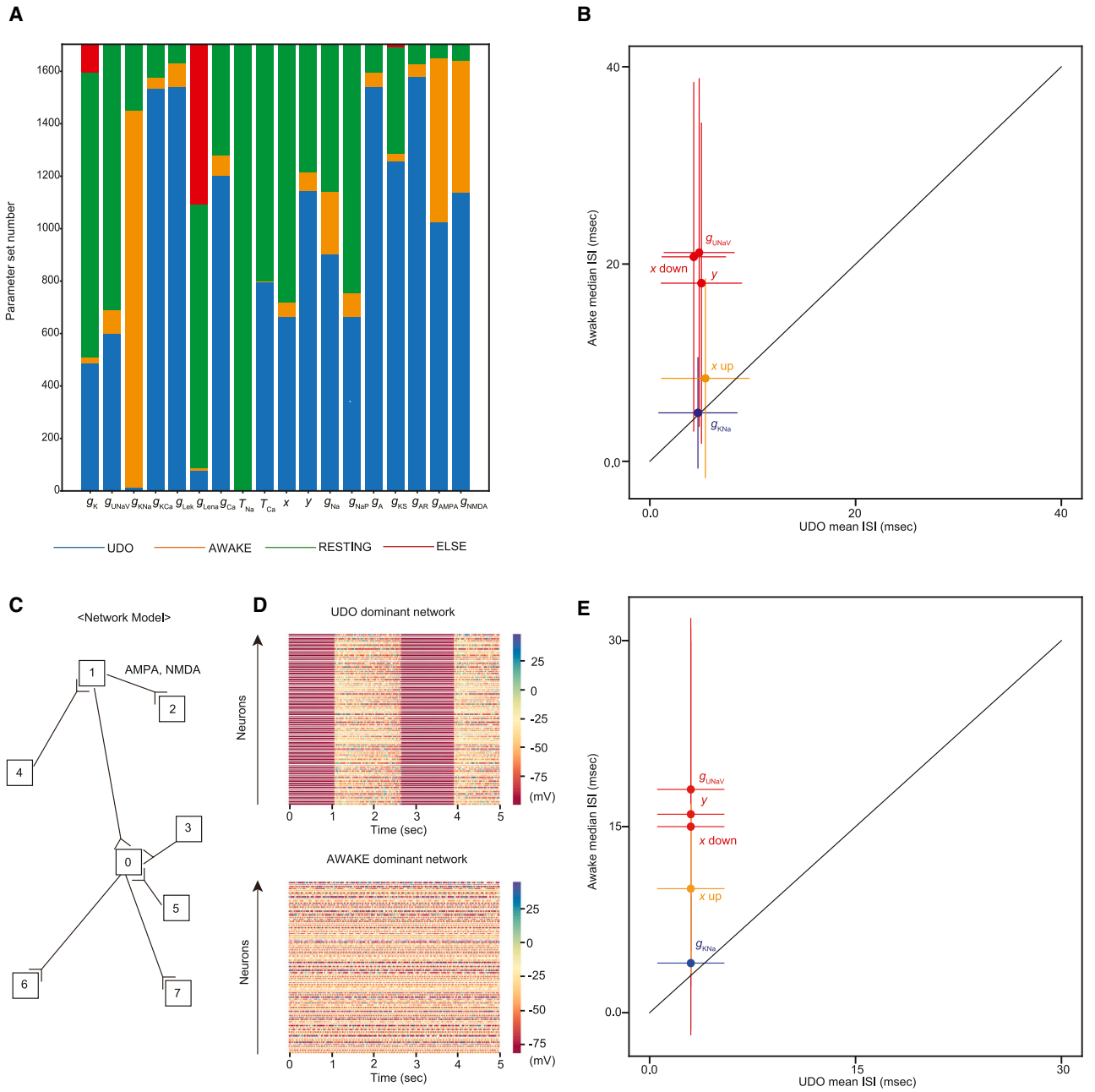

Figure 5. The Full-NAN model shows the importance of the Na^+-dependent hyperpolarization pathway

(A) The result of knockout analysis with all parameter sets inducing UDO. When the contribution of a particular element is set to zero, the number of parameter sets exhibiting the AWAKE firing pattern is indicated by orange, the amount of parameter sets showing the RESTING firing pattern by green, the amount of parameter sets excluded from the analysis (ELSE) owing to their aberrant firing pattern by red, and the amount of parameter sets inducing UDO by blue. The classification criteria of UDO, AWAKE, RESTING, and ELSE follow those of Tatsuki et al. (2016).[11]

(B) The trends of the ISI in the UDO and AWAKE firing pattern. To effectively induce the AWAKE firing pattern for the majority of the parameter sets with UDO, the amount of perturbation was chosen based on the bifurcation analysis in Figure S5A (x, +12.6; y, +14.4; g_{UNaV}, $\times 10^{-0.72}$; g_{KNa}, $\times 10^{-2.0}$). The mean and standard deviation of ISI of the firing pattern are calculated for each parameter set. Dots with color denote the average of the mean ISI of the parameter sets, and bars with color denote the standard deviation of the mean ISI of the parameter sets.

(C) Construction of the network model. The network consists of excitatory neurons. Hence, the neurons are connected with AMPA- or NMDA-mediated synapses.

(D) Representative trace of all neurons in the network model. The upper figure shows a UDO-dominant network, whereas the lower figure shows an AWAKE-dominant network where the conductance of KNa channels is set to be 0.01 times of what it is in the left figure.

(E) Trends of the ISI in the UDO and AWAKE firing patterns. The ISI in UDO in Figure 5F "normal" is compared with the AWAKE firing pattern in Figure 5F "g_{KNa} down," "g_{UNaV} down," "y up," "x down," and "x up." Among the parameter sets showing UDO, changes in the firing pattern from UDO to AWAKE are seen when

(legend continued on next page)

stimulation of neuronal activity-dependent hyperpolarization) and decreased ISI during the up state (through stimulation of the neuronal activity). The activation parameter *x* is also important in shaping the UDO by modulating the Na^+ oscillation period and amplitude (Figure 3A). Having the simulation results recapitulating the tendency of ISI upon the UDO-AWAKE alteration *in vivo* (i.e., the ISI during the up state in UDO tends to be shorter than the ISI in the AWAKE firing pattern), parameter *x* is a candidate point in inducing changes between UDO and AWAKE firing *in vivo* (Figures 3H–3J). The activation/inactivation kinetics of voltage-gated Na^+ channels can be altered by posttranslational modification along with the sleep-wake cycle as several kinases were reported to alter the activation/inactivation kinetics of voltage-gated Na^+ channels.[21,22] Bruning et al. (2019) reported that the phosphorylation level of voltage-gated Na^+ channels increases under the light phase where the mice should have higher sleep needs.[26]

To summarize, posttranslational modification of voltage-gated Na^+ channels and modulation of KNa channels or Na^+/K^+ ATPase in the context of Na^+-dependent hyperpolarization pathway can be regulator of UDO *in vivo*, which are important targets for experimental investigation based on this scheme.

The reversal potential of each ion in our model is approximated as a constant value, as in previous studies.[11,13,14] To explore the possible contribution of the dynamic change in the reversal potential and intra/extracellular ion concentrations, we reformulated the model to calculate the reversal potential and consider all the changes in the intra/extracellular ion concentrations. Using the representative parameter set that induced UDO in the original model, we demonstrated that the observed UDO is conserved in the presence of such reformulations (Figure S7A), suggesting that these dynamics, which are newly incorporated in the revised model, have a minimal effect on UDO, at least in the model using the representative parameter set. Similarly to the NAN model, UDO is conserved in the revised NAN model with Na^+/K^+ ATPase, where the dynamic changes in the reversal potential and intra/extracellular ion concentrations are newly incorporated (Figure S7B), and also in the revised FNAN model (Figure S7C).

Comparison with other mathematical models recapitulating UDO

The essence of the NAN model's scheme is that, during the up state, the amount of intracellular Na^+ that can induce the down state with the activation of KNa channels gradually increases, and, during the down state, the amount of intracellular Na^+ gradually decreases. The role of intracellular Na^+ in the NAN model in inducing the down state can be played by other molecules. Previous studies have suggested that intracellular Ca^{2+}[11,13,27–29] is the inducer of the down state. During the up state, Ca^{2+} enters through voltage-gated Ca^{2+} channels, and, when it is accumulated, KCa channels are activated, thereby inducing the down state. During the down state, plasma membrane Ca^{2+} ATPases (Ca^{2+} pumps/exchangers) pump out intracellular Ca^{2+}, reinitiating the up state. Another motif is the voltage-dependent slowly activating K^+ channels,[30] which is gradually activated during the up state and induces the down state, and, as the membrane potential is hyperpolarized during the down state, the channel is gradually inactivated.

The induction of the down state can be achieved via activity-dependent inactivation of the depolarizing current. Voltage-dependent Na^+ channels[31–33] and Ca^{2+}-dependent inactivation of Ca^{2+} channels[34] are reportedly important in inducing the down state. It is important to investigate the relative contribution of the activity-dependent induction of hyperpolarization and inactivation of depolarization for inducing the down state.

Relevance of the Na^+-dependent hyperpolarization pathway with previous studies

Several lines of evidence support the involvement of the Na^+-dependent hyperpolarization pathway in sleep regulation. The bifurcation diagram in Figure 1F shows that the downregulation of KNa currents altered the firing pattern from UDO to AWAKE. One way to achieve the downregulation of KNa currents is to decrease the intracellular K^+ concentration compared with the extracellular K^+ concentration. In other words, lower extracellular K^+ concentration may lead to sleep. This is consistent with the previous study by Ding et al. (2016) showing that, during sleep/anesthesia, the extracellular K^+ concentration falls.[35] The application of artificial cerebrospinal fluid mimicking the cerebrospinal fluid in the sleep state induced sleep *in vivo*, demonstrating the causal effect of extracellular ion condition on sleep.

Figure 3 shows that the alteration of the activation parameter of voltage-gated Na^+ channels is important in inducing UDO. The activation kinetics of voltage-gated Na^+ channels may be dynamically regulated in the sleep-wake cycle, and phosphorylation of voltage-gated Na^+ channels is one candidate for the regulation. The phosphorylation level of one type of voltage-gated Na^+ channel, namely SCN2a1, is increased when sleep need is accumulated by the administration of MK-801, an NMDA receptor antagonist,[36] or during the light phase in which mice typically sleep.[26] The involvement of SCN2a in the sleep control is demonstrated by showing that Scn2a deficiency leads to increased wakefulness and decreased NREM sleep duration.[37] As the regulation of the activation/inactivation kinetics of a voltage-gated Na^+ channel often includes phosphorylation of the channel,[21,22] it is possible that SCN2a phosphorylation leads to the left shift of the activation parameter, thereby inducing sleep, as suggested by our model.

The bifurcation diagram in Figure 4D shows that the downregulation of Na^+/K^+ ATPase currents alters the firing pattern from UDO to AWAKE. This is supported by animal experiments: mice harboring an inactivating mutation in the neuron-specific Na^+/K^+ ATPase $\alpha 3$ subunit exhibit decreased sleep duration.[38]

the value of the parameter is modified in that the majority of the parameter sets exhibit an AWAKE firing pattern instead of UDO. The exact amount of perturbation given to each parameter is determined by the results of the bifurcation analysis in Figure S5A (*x* down, −12.6; *x* up, +12.6; *y*, +14.4; g_{UNaV}, $\times 10^{-0.72}$; g_{KNa}, $\times 10^{-2.0}$). Parameter sets, which show AWAKE firing pattern when each parameter is changed as above, are selected for each parameter's analysis. The mean and standard deviation of ISI of the firing pattern are calculated for each parameter set. Dots with color denote the average of the mean ISI of the parameter sets, and bars with color denote the standard deviation of the mean ISI of the parameter sets. See also Figures S5–S7 and Tables S3–S5.

Also, the injection of ouabain, an inhibitor of Na^+/K^+ ATPases, enhances wakefulness in mice.[39]

Relationship between the Na^+- and Ca^{2+}-dependent hyperpolarization pathways

While the Na^+- and Ca^{2+}-dependent hyperpolarization pathways are common in that they depend on neuronal activity-dependent K^+ currents to induce the down state, they may have some qualitative differences. In the FNAN model where both the Ca^{2+}- and Na^+-dependent pathways are incorporated, only the Na^+-dependent hyperpolarization pathway drives the up-to-down-state transition (Figures 5A and S5A–S5C). In addition, there may be a link that connects these two pathways. When the intracellular Na^+ concentration is increased, the Na^+-Ca^{2+} exchanger (NCX) serves to pump out intracellular Na^+ and allows the transport of extracellular Ca^{2+} to the intracellular environment. This may lead to the cooperative action of the Ca^{2+}- and Na^+-dependent hyperpolarization pathways to induce UDO.

Limitations of the study

The importance of the Na^+-dependent hyperpolarization pathway for sleep requires experimental validation. The NAN model's prediction of the changes in the neuronal firing pattern upon the perturbation toward the Na^+-dependent hyperpolarization pathway (i.e., trend of bifurcation seen in Figure 1F, trend of the up-/down-state duration, and ISI in Figures 3 and 4) would be of particular interest for the assessment.

In the NAN model, we did not explicitly describe the local concentration of Na^+/Ca^{2+} ions. For example, the KCa and KNa channels would sense the ion concentration at the surface of the soma, which is not essentially the same as the cytosolic ion concentration.

The NAN model, which is described by a set of ordinary differential equations, is too complex to be analytically solved. Therefore, our conclusion derived by the model mostly relied on numerical computing. Although we used over 1,000 solutions showing UDO for detailed analysis to ensure the generalizability of the statements, we could not rule out the possibility that some of the conclusions shown herein depend on the specific parameters used in the numerical simulation rather than the structure of the ODEs.

In this study, we revealed the possible relation between the UDO and Na^+-dependent hyperpolarization pathway. *In vivo* phenotype of UDO would be related to the duration of NREM sleep, delta power, and *in vivo* electrophysiological patterns of cortical pyramidal neurons. Therefore, in order to investigate the role of this pathway in the regulation of slow-wave sleep *in vivo*, such UDO-related sleep parameters need to be analyzed in genetic knockout/knockdown animals lacking components in the Na^+-dependent hyperpolarization pathway (e.g., KNa channels, Na^+/K^+ ATPase, and voltage-gated Na^+ channels).

RESOURCE AVAILABILITY

Lead contact

Further information and requests for resources should be directed to and will be fulfilled by Prof. Hiroki R. Ueda with e-mail: uedah-tky@umin.ac.jp.

Materials availability

This study did not generate new materials.

Data and code availability

- All results were produced from deterministic simulations and can be reproduced by using the same parameters.
- All of the code used for simulations and analyses can be found at https://github.com/DSPsleeporg/nanmodel.
- For any additional questions or information, please contact the lead contact.

ACKNOWLEDGMENTS

We would like to thank F. Tatsuki for valuable discussion. This work was supported by a Grant-in-Aid for Scientific Research (S) (JSPS KAKENHI, 18H05270, to H.R.U.), a Grant-in-Aid for Transformative Research Areas (A) (JSPS KAKENHI 24H02305, to K.L.O.), a Grant-in-Aid for Scientific Research (C) (JSPS KAKENHI 23K05738, to K.L.O.), Human Frontier Science Program (HFSP) Research Grant Program (RGP0019/2018, to H.R.U.), Exploratory Research for Advanced Technology (ERATO) (JST, JPMJER2001, to H.R.U.), Quantum Leap Flagship Program (Q-LEAP MEXT, JPMXS0120330644, to H.R.U.), Brain Mapping by Integrated Neurotechnologies for Disease Studies (Brain/MINDS) (AMED, JP21dm0207049, to H.R.U.), Innovative Drug Discovery and Development (AMED, JP19am0401011, to H.R.U.), and an intra-mural Grant-in-Aid (RIKEN BDR, to H.R.U.). We would like to thank Enago (www.enago.jp) for the English language review.

AUTHOR CONTRIBUTIONS

T.R.S., K.L.O., and H.R.U. designed the study. T.R.S. performed most of the simulation study. F.L.K. and T.R.S. wrote the code for the network simulation. T.R.S., K.L.O., and H.R.U. analyzed the mechanism of UDO. T.R.S., K.L.O., and H.R.U. wrote the manuscript.

DECLARATION OF INTERESTS

H.R.U. is a member of iScience's editorial advisory board.

STAR★METHODS

Detailed methods are provided in the online version of this paper and include the following:

- KEY RESOURCES TABLE
- EXPERIMENTAL MODEL AND STUDY PARTICIPANT DETAILS
- METHOD DETAILS
  - Formulation of several mathematical models for up–down oscillation with Na^+ dynamics
  - Parameter search
  - Bifurcation analysis
  - Plotting the normalized voltage (V) and [Na^+]
  - Choosing the representative parameter set
  - Plotting the intersection of nullplanes
  - Measuring the up-state duration, down-state duration, Na^+ oscillation amplitude, and ISI
  - Construction of the network model
- QUANTIFICATION AND STATISTICAL ANALYSIS

SUPPLEMENTAL INFORMATION

Supplemental information can be found online at https://doi.org/10.1016/j.isci.2025.111904.

Received: August 5, 2024
Revised: December 10, 2024
Accepted: January 23, 2025
Published: January 27, 2025

REFERENCES

1. Walter, W.G. (1937). The Electro-encephalogram in Cases of Cerebral Tumour: (Section of Neurology). Proc. R. Soc. Med. *30*, 579–598.
2. Steriade, M., Timofeev, I., and Grenier, F. (2001). Natural waking and sleep states: a view from inside neocortical neurons. J. Neurophysiol. *85*, 1969–1985. https://doi.org/10.1152/jn.2001.85.5.1969.
3. Steriade, M. (2003). The corticothalamic system in sleep. Front. Biosci. *8*, d878–d899. https://doi.org/10.2741/1043.
4. Wilson, C.J., and Kawaguchi, Y. (1996). The origins of two-state spontaneous membrane potential fluctuations of neostriatal spiny neurons. J. Neurosci. *16*, 2397–2410. https://doi.org/10.1523/JNEUROSCI.16-07-02397.1996.
5. Hindmarsh, J.L., and Rose, R.M. (1984). A model of neuronal bursting using three coupled first order differential equations. Proc. R. Soc. Lond. B Biol. Sci. *221*, 87–102. https://doi.org/10.1098/rspb.1984.0024.
6. Hill, S., and Tononi, G. (2005). Modeling sleep and wakefulness in the thalamocortical system. J. Neurophysiol. *93*, 1671–1698. https://doi.org/10.1152/jn.00915.2004.
7. Sanchez-Vives, M.V., Mattia, M., Compte, A., Perez-Zabalza, M., Winograd, M., Descalzo, V.F., and Reig, R. (2010). Inhibitory modulation of cortical up states. J. Neurophysiol. *104*, 1314–1324. https://doi.org/10.1152/jn.00178.2010.
8. Timofeev, I., Grenier, F., Bazhenov, M., Sejnowski, T.J., and Steriade, M. (2000). Origin of slow cortical oscillations in deafferented cortical slabs. Cerebr. Cortex *10*, 1185–1199. https://doi.org/10.1093/cercor/10.12.1185.
9. Xu, Y., Ma, J., Zhan, X., Yang, L., and Jia, Y. (2019). Temperature effect on memristive ion channels. Cogn. Neurodyn. *13*, 601–611. https://doi.org/10.1007/s11571-019-09547-8.
10. Vazquez-Guerrero, P., Tuladhar, R., Psychalinos, C., Elwakil, A., Chacron, M.J., and Santamaria, F. (2024). Fractional order memcapacitive neuromorphic elements reproduce and predict neuronal function. Sci. Rep. *14*, 5817. https://doi.org/10.1038/s41598-024-55784-1.
11. Tatsuki, F., Sunagawa, G.A., Shi, S., Susaki, E.A., Yukinaga, H., Perrin, D., Sumiyama, K., Ukai-Tadenuma, M., Fujishima, H., Ohno, R.i., et al. (2016). Involvement of Ca(2+)-Dependent Hyperpolarization in Sleep Duration in Mammals. Neuron *90*, 70–85. https://doi.org/10.1016/j.neuron.2016.02.032.
12. HODGKIN, A.L., and HUXLEY, A.F. (1952). A quantitative description of membrane current and its application to conduction and excitation in nerve. J. Physiol. *117*, 500–544. https://doi.org/10.1113/jphysiol.1952.sp004764.
13. Yoshida, K., Shi, S., Ukai-Tadenuma, M., Fujishima, H., Ohno, R.I., and Ueda, H.R. (2018). Leak potassium channels regulate sleep duration. Proc. Natl. Acad. Sci. USA *115*, E9459–E9468. https://doi.org/10.1073/pnas.1806486115.
14. Compte, A., Sanchez-Vives, M.V., McCormick, D.A., and Wang, X.J. (2003). Cellular and network mechanisms of slow oscillatory activity (<1 Hz) and wave propagations in a cortical network model. J. Neurophysiol. *89*, 2707–2725. https://doi.org/10.1152/jn.00845.2002.
15. Brown, M.R., Kronengold, J., Gazula, V.R., Spilianakis, C.G., Flavell, R.A., von Hehn, C.A.A., Bhattacharjee, A., and Kaczmarek, L.K. (2008). Amino-termini isoforms of the Slack K+ channel, regulated by alternative promoters, differentially modulate rhythmic firing and adaptation. J. Physiol. *586*, 5161–5179. https://doi.org/10.1113/jphysiol.2008.160861.
16. Kaczmarek, L.K. (2013). Slack, Slick and Sodium-Activated Potassium Channels. ISRN Neurosci. *2013*, 354262. https://doi.org/10.1155/2013/354262.
17. Kiss, T. (2008). Persistent Na-channels: origin and function. A review. Acta Biol. Hung. *59*, 1–12. https://doi.org/10.1556/ABiol.59.2008.Suppl.1.
18. Fleidervish, I.A., Friedman, A., and Gutnick, M.J. (1996). Slow inactivation of Na+ current and slow cumulative spike adaptation in mouse and guinea-pig neocortical neurones in slices. J. Physiol. *493*, 83–97. https://doi.org/10.1113/jphysiol.1996.sp021366.
19. Kaplan, J.H. (2002). Biochemistry of Na,K-ATPase. Annu. Rev. Biochem. *71*, 511–535. https://doi.org/10.1146/annurev.biochem.71.102201.141218.
20. Kager, H., Wadman, W.J., and Somjen, G.G. (2000). Simulated seizures and spreading depression in a neuron model incorporating interstitial space and ion concentrations. J. Neurophysiol. *84*, 495–512. https://doi.org/10.1152/jn.2000.84.1.495.
21. Thompson, C.H., Hawkins, N.A., Kearney, J.A., and George, A.L. (2017). CaMKII modulates sodium current in neurons from epileptic. Proc. Natl. Acad. Sci. USA *114*, 1696–1701. https://doi.org/10.1073/pnas.1615774114.
22. Dascal, N., and Lotan, I. (1991). Activation of protein kinase C alters voltage dependence of a Na+ channel. Neuron *6*, 165–175. https://doi.org/10.1016/0896-6273(91)90131-i.
23. Watson, B.O., Levenstein, D., Greene, J.P., Gelinas, J.N., and Buzsáki, G. (2016). Network Homeostasis and State Dynamics of Neocortical Sleep. Neuron *90*, 839–852. https://doi.org/10.1016/j.neuron.2016.03.036.
24. Gagnon, K.B., and Delpire, E. (2020). Sodium Transporters in Human Health and Disease. Front. Physiol. *11*, 588664. https://doi.org/10.3389/fphys.2020.588664.
25. Wu, S.N., Yeh, C.C., Huang, H.C., So, E.C., and Lo, Y.C. (2012). Electrophysiological characterization of sodium-activated potassium channels in NG108-15 and NSC-34 motor neuron-like cells. Acta Physiol. *206*, 120–134. https://doi.org/10.1111/j.1748-1716.2012.02438.x.
26. Brüning, F., Noya, S.B., Bange, T., Koutsouli, S., Rudolph, J.D., Tyagarajan, S.K., Cox, J., Mann, M., Brown, S.A., and Robles, M.S. (2019). Sleep-wake cycles drive daily dynamics of synaptic phosphorylation. Science *366*, eaav3617. https://doi.org/10.1126/science.aav3617.
27. Fridlyand, L.E., Tamarina, N., and Philipson, L.H. (2010). Bursting and calcium oscillations in pancreatic beta-cells: specific pacemakers for specific mechanisms. Am. J. Physiol. Endocrinol. Metab. *299*, E517–E532. https://doi.org/10.1152/ajpendo.00177.2010.
28. Traub, R.D., Wong, R.K., Miles, R., and Michelson, H. (1991). A model of a CA3 hippocampal pyramidal neuron incorporating voltage-clamp data on intrinsic conductances. J. Neurophysiol. *66*, 635–650. https://doi.org/10.1152/jn.1991.66.2.635.
29. Stanford, I.M., Traub, R.D., and Jefferys, J.G. (1998). Limbic gamma rhythms. II. Synaptic and intrinsic mechanisms underlying spike doublets in oscillating subicular neurons. J. Neurophysiol. *80*, 162–171. https://doi.org/10.1152/jn.1998.80.1.162.
30. Wang, X.J. (1999). Fast burst firing and short-term synaptic plasticity: a model of neocortical chattering neurons. Neuroscience *89*, 347–362. https://doi.org/10.1016/s0306-4522(98)00315-7.
31. Huguenard, J.R., and McCormick, D.A. (1992). Simulation of the currents involved in rhythmic oscillations in thalamic relay neurons. J. Neurophysiol. *68*, 1373–1383. https://doi.org/10.1152/jn.1992.68.4.1373.
32. Butera, R.J., Rinzel, J., and Smith, J.C. (1999). Models of respiratory rhythm generation in the pre-Bötzinger complex. I. Bursting pacemaker neurons. J. Neurophysiol. *82*, 382–397. https://doi.org/10.1152/jn.1999.82.1.382.
33. Destexhe, A., Contreras, D., Sejnowski, T.J., and Steriade, M. (1994). A model of spindle rhythmicity in the isolated thalamic reticular nucleus. J. Neurophysiol. *72*, 803–818. https://doi.org/10.1152/jn.1994.72.2.803.
34. Canavier, C.C., Clark, J.W., and Byrne, J.H. (1991). Simulation of the bursting activity of neuron R15 in Aplysia: role of ionic currents, calcium balance, and modulatory transmitters. J. Neurophysiol. *66*, 2107–2124. https://doi.org/10.1152/jn.1991.66.6.2107.
35. Ding, F., O'Donnell, J., Xu, Q., Kang, N., Goldman, N., and Nedergaard, M. (2016). Changes in the composition of brain interstitial ions control the sleep-wake cycle. Science *352*, 550–555. https://doi.org/10.1126/science.aad4821.

36. Wang, Z., Ma, J., Miyoshi, C., Li, Y., Sato, M., Ogawa, Y., Lou, T., Ma, C., Gao, X., Lee, C., et al. (2018). Quantitative phosphoproteomic analysis of the molecular substrates of sleep need. Nature *558*, 435–439. https://doi.org/10.1038/s41586-018-0218-8.

37. Ma, Z., Eaton, M., Liu, Y., Zhang, J., Chen, X., Tu, X., Shi, Y., Que, Z., Wettschurack, K., Zhang, Z., et al. (2022). Deficiency of autism-related Scn2a gene in mice disrupts sleep patterns and circadian rhythms. Neurobiol. Dis. *168*, 105690. https://doi.org/10.1016/j.nbd.2022.105690.

38. Kirshenbaum, G.S., Clapcote, S.J., Duffy, S., Burgess, C.R., Petersen, J., Jarowek, K.J., Yücel, Y.H., Cortez, M.A., Snead, O.C., Vilsen, B., et al. (2011). Mania-like behavior induced by genetic dysfunction of the neuron-specific Na+,K+-ATPase α3 sodium pump. Proc. Natl. Acad. Sci. USA *108*, 18144–18149. https://doi.org/10.1073/pnas.1108416108.

39. Lelkes, Z. (2020). Ouabain, a Na-K-ATPase inhibitor, enhances wakefulness in rats. Neuropharmacology *176*, 108224. https://doi.org/10.1016/j.neuropharm.2020.108224.

40. Bazhenov, M., Timofeev, I., Steriade, M., and Sejnowski, T.J. (2002). Model of thalamocortical slow-wave sleep oscillations and transitions to activated States. J. Neurosci. *22*, 8691–8704. https://doi.org/10.1523/JNEUROSCI.22-19-08691.2002.

41. Chen, J.Y., Chauvette, S., Skorheim, S., Timofeev, I., and Bazhenov, M. (2012). Interneuron-mediated inhibition synchronizes neuronal activity during slow oscillation. J. Physiol. *590*, 3987–4010. https://doi.org/10.1113/jphysiol.2012.227462.

42. Sabatini, B.L., Oertner, T.G., and Svoboda, K. (2002). The life cycle of Ca(2+) ions in dendritic spines. Neuron *33*, 439–452. https://doi.org/10.1016/s0896-6273(02)00573-1.

43. Lu, B., Su, Y., Das, S., Liu, J., Xia, J., and Ren, D. (2007). The neuronal channel NALCN contributes resting sodium permeability and is required for normal respiratory rhythm. Cell *129*, 371–383. https://doi.org/10.1016/j.cell.2007.02.041.

44. EDSTROM, J.E. (1957). Effects of increased motor activity on the dimensions and the staining properties of the neuron soma. J. Comp. Neurol. *107*, 295–304. https://doi.org/10.1002/cne.901070207.

45. Chen, K.C., and Nicholson, C. (2000). Spatial buffering of potassium ions in brain extracellular space. Biophys. J. *78*, 2776–2797. https://doi.org/10.1016/S0006-3495(00)76822-6.

STAR★METHODS

KEY RESOURCES TABLE

REAGENT or RESOURCE	SOURCE	IDENTIFIER
Software and algorithms		
C++17	ISO	https://isocpp.org/
CUDA 11.8	NVIDIA	https://developer.nvidia.com/cuda-toolkit
Python 3.7.0	Python Software Foundation	https://www.python.org/
scikit-learn 1.3.2	scikit-learn	https://scikit-learn.org/
SciPy 1.1.0 or 1.5.2	SciPy	https://scipy.org/
Scripts for simulations and analyses	This paper	https://github.com/DSPsleeporg/nanmodel

EXPERIMENTAL MODEL AND STUDY PARTICIPANT DETAILS

This study used mathematical models and did not use any biological samples.

METHOD DETAILS

Formulation of several mathematical models for up–down oscillation with Na^+ dynamics

The models and parameters used in this study are based on the AN model.[11] The AN model is constructed based on previous studies[6–8,14,40,41] using the Hodgkin–Huxley-type equations.

The NAN model, NAN model without a voltage-gated Ca^{2+} channel, NAN model with Na^+/K^+ ATPase, and FNAN model are constructed as follows:

The formula for the NAN model is as follows:

$$CA\frac{dV}{dt} = -A(I_{Leak} + I_K + I_{UNaV} + I_{KNa} + I_{Ca}) \quad \text{(Equation 8)}$$

The formula for the NAN model without a voltage-gated Ca^{2+} channel is as follows:

$$CA\frac{dV}{dt} = -A(I_{Leak} + I_K + I_{UNaV} + I_{KNa}) \quad \text{(Equation 9)}$$

The formula for the NAN model with Na^+/K^+ ATPase is as follows:

$$CA\frac{dV}{dt} = -A(I_{Leak} + I_K + I_{UNaV} + I_{NaK} + I_{Ca}) \quad \text{(Equation 10)}$$

The formula for the FNAN model is as follows:

$$CA\frac{dV}{dt} = -A(I_{Leak} + I_K + I_{UNaV} + I_{KNa} + I_{Ca} + I_{Na} + I_A + I_{KS} + I_{KCa} + I_{NaP} + I_{AR}) - I_{NMDA} - I_{AMPA} - I_{GABA} \quad \text{(Equation 11)}$$

For all the models, C denotes the membrane capacitance; A, the area of a single neuron; V, the membrane potential; and I, the electric current of each channel. The other parameters used in this study are listed in Tables S1–S5. Each intrinsic current is given in Equations 12, 13, 14, 15, 16, 17, 18, 19, 20, 21, 22, 23, 24, 25, 26, 27, 28, 29, 30, 31, 32, 33, 34, 35, 36, 37, 38, 39, 40, 41, 42, 43, 44, 45, 46, 47, 48, 49, 50, 51, and 52:

$$I_{LeNa} = g_{LeNa}(V - V_{LeNa}) \quad \text{(Equation 12)}$$

$$I_{LeK} = g_{LeK}(V - V_K) \quad \text{(Equation 13)}$$

$$I_{Leak} = g_{Leak}(V - V_{Leak}) = I_{LeNa} + I_{LeK} \quad \text{(Equation 14)}$$

$$g_{LeNa} = g_{Leak}\frac{V_{Leak} - V_{LeNa}}{V_K - V_{LeNa}} \quad \text{(Equation 15)}$$

$$g_{LeK} = g_{Leak}\frac{V_{Leak} - V_K}{V_{LeNa} - V_K} \quad \text{(Equation 16)}$$

$$I_K = g_K n_K{}^4 (V - V_K) \quad \text{(Equation 17)}$$

$$\frac{dn_K}{dt} = 4(\alpha_n(1 - n_K) - \beta_n n_K) \quad \text{(Equation 18)}$$

$$\alpha_n = 0.01(V + 34)/\left[1 - exp(-(V + 34)/10)\right] \quad \text{(Equation 19)}$$

$$\beta_n = 0.125\, exp\,(-(V + 44)/25) \quad \text{(Equation 20)}$$

$$I_{KNa} = g_{KNa} m_{KNa}\,(V - V_K) \quad \text{(Equation 21)}$$

$$m_{KNa} = 1 \Big/ \left[1 + (Ke/[Na^+])^{Kf}\right] \quad \text{(Equation 22)}$$

$$I_{Ca} = g_{Ca} m_{Ca}{}^2 (V - V_{Ca}) \quad \text{(Equation 23)}$$

$$m_{Ca} = 1/[1 + exp(-(V + 20)/9)] \quad \text{(Equation 24)}$$

$$I_{UNaV} = g_{UNaV} m_{UNaV}{}^3 h_{UNaV} (V - V_{Na}) \quad \text{(Equation 25)}$$

$$m_{UNaV} = \alpha_m/(\alpha_m + \beta_m) \quad \text{(Equation 26)}$$

$$\alpha_m = 0.1(V + 33 + x)/\left[1 - exp(-(V + 33 + x)/10\right] \quad \text{(Equation 27)}$$

$$\beta_m = 4\, exp(-(V + 53.7 + x)/12) \quad \text{(Equation 28)}$$

$$\frac{dh_{UNaV}}{dt} = 4\,(\alpha_h\,(1 - h_{UNaV}) - \beta_h\, h_{UNaV}) \quad \text{(Equation 29)}$$

$$\alpha_h = 0.07\, exp\,(-(V + 50 + y)/10) \quad \text{(Equation 30)}$$

$$\beta_h = 1/\left[1 + exp\,(-(V + 20 + y)/10)\right] \quad \text{(Equation 31)}$$

$$I_{NaK} = g_{NaK}\left[\left(1+\frac{3.5}{4.0}\right)^{-3}\right]\left[\left(1+\frac{10.0}{[Na^+]}\right)^{-2}\right] \quad \text{(Equation 32)}$$

$$I_{Na} = g_{Na}\, m_{Na}{}^3 h_{Na} (V - V_{Na}) \quad \text{(Equation 33)}$$

$$m_{Na} = \alpha_m/(\alpha_m + \beta_m) \quad \text{(Equation 34)}$$

$$\alpha_m = 0.1\,(V + 33)/\left[1 - exp\,(-(V + 33)/10\right] \quad \text{(Equation 35)}$$

$$\beta_m = 4\, exp\,(-(V + 53.7)/12) \quad \text{(Equation 36)}$$

$$\frac{dh_{Na}}{dt} = 4\,(\alpha_h(1 - h_{Na}) - \beta_h\, h_{Na}) \quad \text{(Equation 37)}$$

$$\alpha_h = 0.07\, exp\,(-(V+50)/10) \quad \text{(Equation 38)}$$

$$\beta_h = 1/[1+exp\,(-(V+20)/10)] \quad \text{(Equation 39)}$$

$$I_A = g_A\, m_A{}^3\, h_A\,(V - V_K) \quad \text{(Equation 40)}$$

$$m_A = 1/[1+exp(-(V+44)/50)] \quad \text{(Equation 41)}$$

$$\frac{dh_A}{dt} = \frac{(h_{A\infty} - h_A)}{\tau_{h_A}} \quad \text{(Equation 42)}$$

$$h_{A\infty} = 1/[1+exp(-(V+80)/6)] \quad \text{(Equation 43)}$$

$$I_{KS} = g_{KS}\, m_{KS}\,(V - V_K) \quad \text{(Equation 44)}$$

$$\frac{dm_{KS}}{dt} = (m_{KS\infty} - m_{KS}) \Big/ \tau_{m_{KS}} \quad \text{(Equation 45)}$$

$$m_{KS\infty} = 1/[1+exp(-(V+34)/6.5)] \quad \text{(Equation 46)}$$

$$\tau_{m_{KS}} = 8/[exp(-(V+55)/30) + exp((V+55)/30)] \quad \text{(Equation 47)}$$

$$I_{KCa} = g_{KCa} m_{KCa}\,(V - V_K) \quad \text{(Equation 48)}$$

$$m_{KCa} = 1 \Big/ \left[1 + \left(Kd \Big/ \left[Ca^{2+}\right]\right)^{3.5}\right] \quad \text{(Equation 49)}$$

$$I_{NaP} = g_{NaP}\, m_{NaP\infty}{}^3 (V - V_{Na}) \quad \text{(Equation 50)}$$

$$m_{NaP\infty} = 1/[1+exp(-(V+55.7)/7.7)] \quad \text{(Equation 51)}$$

$$I_{AR} = g_{AR}\, h_{AR\infty}\,(V - V_K) \quad \text{(Equation 52)}$$

$$h_{AR\infty} = 1/[1+exp(-(V+75)/4)] \quad \text{(Equation 53)}$$

Note that *Ke* and *Kf* in the formula of the KNa channels (22) are fitted based on the activation curve (Figure 2B in the previous study).[16] The formulation of the current mediated by Na^+/K^+ ATPases (32) is incorporated from the previous study.[20]

In the FNAN model, the description of synaptic elements is altered from the AN model so that they influence the membrane potential but not the intracellular ion concentration. This assumption is different from that in the AN model that synaptic currents alter the intracellular ionic concentration.[11] This is because a previous study reported that the ionic diffusion across the spine is negligible[42] and that the spine head functions as a separate compartment from the soma. Therefore, in the FNAN model, the actions of NMDAR and AMPAR are described to be unrelated to intracellular Na^+ dynamics and that NMDAR is unrelated to intracellular Ca^{2+} dynamics. Each extrinsic current is given by Equations 54, 55, 56, 57, 58, 59, 60, 61, 62, and 63:

$$I_{AMPA} = g_{AMPA}\, s_{AMPA}\,(V - V_{AMPA}) \quad \text{(Equation 54)}$$

$$\frac{ds_{AMPA}}{dt} = 3.48 f(V) - \frac{s_{AMPA}}{\tau_{AMPA}} \quad \text{(Equation 55)}$$

$$f(V) = 1/[1+exp(-(V-20)/2)] \quad \text{(Equation 56)}$$

$$I_{NMDA} = g_{NMDA}\, s_{NMDA}\, (V - V_{NMDA}) \quad \text{(Equation 57)}$$

$$\frac{ds_{NMDA}}{dt} = 0.5 x_{NMDA}\, (1 - s_{NMDA}) - \frac{s_{NMDA}}{x_{NMDA}} \quad \text{(Equation 58)}$$

$$\frac{dx_{NMDA}}{dt} = 3.48\, f(V) - \frac{x_{NMDA}}{\tau_{x_{NMDA}}} \quad \text{(Equation 59)}$$

$$f(V) = 1/[1 + exp(-(V - 20)/2)] \quad \text{(Equation 60)}$$

$$I_{GABA} = g_{GABA}\, s_{GABA}\, (V - V_{GABA}) \quad \text{(Equation 61)}$$

$$\frac{ds_{GABA}}{dt} = f(V) - \frac{s_{GABA}}{\tau_{GABA}} \quad \text{(Equation 62)}$$

$$f(V) = 1/[1 + exp(-(V - 20)/2)] \quad \text{(Equation 63)}$$

Leak Na channels (NALCN channels) allow Na^+, K^+, and Ca^{2+} currents.[43] Therefore, the leak Na^+ current can be divided into Na^+, K^+, and Ca^{2+} currents as follows:

$$I_{LeNa} = I_{Na-NALCN} + I_{K-NALCN} + I_{Ca-NALCN} \quad \text{(Equation 64)}$$

$$I_{Na-NALCN} = g_{Na-NALCN}(V - V_{Na}) \quad \text{(Equation 65)}$$

$$I_{K-NALCN} = g_{K-NALCN}(V - V_K) \quad \text{(Equation 66)}$$

$$I_{Ca-NALCN} = g_{Ca-NALCN}(V - V_{Ca}) \quad \text{(Equation 67)}$$

These must satisfy the following equation:

$$g_{LeNa} = g_{Na-NALCN} + g_{K-NALCN} + g_{Ca-NALCN} \quad \text{(Equation 68)}$$

To determine the proportion of $g_{Na-NALCN}$, $g_{K-NALCN}$, and $g_{Ca-NALCN}$, electrophysiological recordings of NALCN channels are used.[43] Suppose that the reversal potential of NALCN channels is γ_1 mV when $[Na^+]_o = 155$ mM.[43] Suppose that the reversal potential of NALCN channels is γ_2 mV when $[Na^+]_o = 15.5$ mM.[43] Assuming that the reversal potential of Na^+ is V_{Na1} when $[Na^+]_o = 155$ mM and the reversal potential of Na^+ is V_{Na2} when $[Na^+]_o = 15.5$ mM, based on the definition of reversal potential, the following equations hold:

$$\gamma_1 = (g_{Ca-NALCN}V_{Ca} + g_{K-NALCN}V_K + g_{Na-NALCN}V_{Na1}) / (g_{Na-NALCN} + g_{K-NALCN} + g_{Ca-NALCN}) \quad \text{(Equation 69)}$$

$$\gamma_2 = (g_{Ca-NALCN}V_{Ca} + g_{K-NALCN}V_K + g_{Na-NALCN}V_{Na2}) / (g_{Na-NALCN} + g_{K-NALCN} + g_{Ca-NALCN}) \quad \text{(Equation 70)}$$

Therefore,

$$\gamma_1 - \gamma_2 = \{g_{Na-NALCN} / (g_{Na-NALCN} + g_{K-NALCN} + g_{Ca-NALCN})\}(V_{Na1} - V_{Na2}) \quad \text{(Equation 71)}$$

$$V_{Na1} = 26.3\, ln \frac{155}{[Na^+]_i} \quad \text{(Equation 72)}$$

$$V_{Na2} = 26.3\, ln \frac{15.5}{[Na^+]_i} \quad \text{(Equation 73)}$$

Therefore,

$$V_{Na1} - V_{Na2} = 26.3\, ln \frac{155}{15.5} = 26.3\, ln\, 10 \quad \text{(Equation 74)}$$

Therefore,

$$g_{Na-NALCN} = (\gamma_1 - \gamma_2)(g_{Na-NALCN} + g_{K-NALCN} + g_{Ca-NALCN}) / 26.3\, ln\, 10 \quad \text{(Equation 75)}$$

Suppose that the reversal potential of NALCN channels is δ_1 mV when $[K^+]_o$ = 155 mM.[43] Suppose that the reversal potential of NALCN channels is δ_2 mV when $[K^+]_o$ = 15.5 mM.[43] Assuming that the reversal potential of K^+ is V_{K1} when $[K^+]_o$ = 155 mM and the reversal potential of K^+ is V_{K2} when $[K^+]_o$ = 15.5 mM, based on the definition of reversal potential, the following equations hold:

$$\delta_1 = (g_{Ca-NALCN}V_{Ca} + g_{K-NALCN}V_{K1} + g_{Na-NALCN}V_{Na}) / (g_{Na-NALCN} + g_{K-NALCN} + g_{Ca-NALCN}) \quad \text{(Equation 76)}$$

$$\delta_2 = (g_{Ca-NALCN}V_{Ca} + g_{K-NALCN}V_{K2} + g_{Na-NALCN}V_{Na}) / (g_{Na-NALCN} + g_{K-NALCN} + g_{Ca-NALCN}) \quad \text{(Equation 77)}$$

Therefore,

$$\delta_1 - \delta_2 = \{g_{K-NALCN} / (g_{Na-NALCN} + g_{K-NALCN} + g_{Ca-NALCN})\}(V_{K1} - V_{K2}) \quad \text{(Equation 78)}$$

$$V_{K1} = 26.3\, ln \frac{155}{[K^+]_i} \quad \text{(Equation 79)}$$

$$V_{K2} = 26.3\, ln \frac{15.5}{[K^+]_i} \quad \text{(Equation 80)}$$

Therefore,

$$V_{K1} - V_{K2} = 26.3\, ln \frac{155}{15.5} = 26.3\, ln\, 10 \quad \text{(Equation 81)}$$

Therefore,

$$g_{K-NALCN} = (\delta_1 - \delta_2)(g_{Na-NALCN} + g_{K-NALCN} + g_{Ca-NALCN}) / 26.3\, ln\, 10 \quad \text{(Equation 82)}$$

Suppose that the reversal potential of NALCN channels is ϵ_1 mV when $[Ca^{2+}]_o$ = 100 mM.[43] Suppose that the reversal potential of NALCN channels is ϵ_2 mV when $[Ca^{2+}]_o$ = 10 mM.[43] Assuming that the reversal potential of Ca^{2+} is V_{Ca1} when $[Ca^{2+}]_o$ = 100 mM and the reversal potential of Ca^{2+} is V_{Ca2} when $[Ca^{2+}]_o$ = 10 mM, based on the definition of reversal potential, the following equations hold:

$$\epsilon_1 = (g_{Ca-NALCN}V_{Ca1} + g_{K-NALCN}V_K + g_{Na-NALCN}V_{Na}) / (g_{Na-NALCN} + g_{K-NALCN} + g_{Ca-NALCN}) \quad \text{(Equation 83)}$$

$$\epsilon_2 = (g_{Ca-NALCN}V_{Ca2} + g_{K-NALCN}V_K + g_{Na-NALCN}V_{Na}) / (g_{Na-NALCN} + g_{K-NALCN} + g_{Ca-NALCN}) \quad \text{(Equation 84)}$$

Therefore,

$$\epsilon_1 - \epsilon_2 = \{g_{Ca-NALCN} / (g_{Na-NALCN} + g_{K-NALCN} + g_{Ca-NALCN})\}(V_{Ca1} - V_{Ca2}) \quad \text{(Equation 85)}$$

$$V_{Ca1} = 26.3\, ln \frac{100}{[Ca^{2+}]_i} \quad \text{(Equation 86)}$$

$$V_{Ca2} = 26.3\, ln \frac{10}{[Ca^{2+}]_i} \quad \text{(Equation 87)}$$

Therefore,

$$V_{Ca1} - V_{Ca2} = 26.3\, ln \frac{100}{10} = 26.3\, ln\, 10 \quad \text{(Equation 88)}$$

Therefore,

$$g_{Ca-NALCN} = (\epsilon_1 - \epsilon_2)(g_{Na-NALCN} + g_{K-NALCN} + g_{Ca-NALCN}) / 26.3\, ln\, 10 \quad \text{(Equation 89)}$$

Based on Equations 75, 82, and 89, the proportions of $g_{Na\text{-}NALCN}$, $g_{K\text{-}NALCN}$, and $g_{Ca\text{-}NALCN}$ are determined as follows:

$$g_{Na-NALCN} : g_{K-NALCN} : g_{Ca-NALCN} = (\gamma_1 - \gamma_2) : (\delta_1 - \delta_2) : (\epsilon_1 - \epsilon_2) \quad \text{(Equation 90)}$$

γ_1 = 10.89, γ_2 = − 34.65, δ_1 = 11.76, δ_2 = − 20.79, ϵ_1 = 16.00, ϵ_2 = − 9.80[43]

Therefore,

$$g_{Na-NALCN} : g_{K-NALCN} : g_{Ca-NALCN} = 45.54 : 32.55 : 25.80 \quad \text{(Equation 91)}$$

Therefore,

$$g_{Na-NALCN} = 0.44 g_{LeNa} \quad \text{(Equation 92)}$$

$$g_{K-NALCN} = 0.31 g_{LeNa} \quad \text{(Equation 93)}$$

$$g_{Ca-NALCN} = 0.25 g_{LeNa} \quad \text{(Equation 94)}$$

The time course of the intracellular Na^+ concentration is also modeled as follows:
The formulas for the NAN model and the NAN model without a voltage-gated Ca^{2+} channel are as follows:

$$\frac{d[Na^+]}{dt} = -\alpha_{Na} A(I_{UNaV} + I_{Na-NALCN}) - \frac{[Na^+]}{\tau_{Na}} \quad \text{(Equation 95)}$$

The formulas for the NAN model and the NAN model with Na^+/K^+ ATPase are follows:

$$\frac{d[Na^+]}{dt} = -\alpha_{Na} A(I_{UNaV} + I_{Na-NALCN} - 3I_{NaK}) \quad \text{(Equation 96)}$$

The formula for the FNAN model is as follows:

$$\frac{d[Na^+]}{dt} = -\alpha_{Na} A(I_{Na} + I_{NaP} + I_{UNaV} + I_{Na-NALCN}) - \frac{[Na^+]}{\tau_{Na}} \quad \text{(Equation 97)}$$

The time course of the intracellular Ca^{2+} concentration in the FNAN model was also modeled as follows:

$$\frac{d[Ca^{2+}]}{dt} = -\alpha_{Ca} A(I_{Ca} + I_{Ca-NALCN}) - \frac{[Ca^{2+}]}{\tau_{Ca}} \quad \text{(Equation 98)}$$

The coefficient of Na^+-entry (αNa) is estimated under the assumption that the average volume of a single neuron is ~10 pL.[44] The increase in intracellular Na^+ concentration caused by the Na^+ currents was determined as follows: 1-nA Na^+ current for 1 ms causes 1 nA × 1 ms/~10 pL = 1 pC/~10 pL = ~1.0/10 F mol/L = ~1.0 μM increase in the intracellular Na^+ concentration, where F = ~0.96 × 10^5 C/mol is the Faraday constant.

Integration is performed with the following initial values in each parameter search and bifurcation analysis: V = −45 mV, h_{NaV} = 0.045 (unitless), h_{UNaV} = 0.045 (unitless), n_K = 0.54 (unitless), [Na^+] = 1 mM.

The coefficient of Na^+-entry (αNa) is estimated under the assumption that the average volume of a single neuron is ~10 pL.[44] The increase in intracellular Na^+ concentration caused by Na^+ currents was determined as follows: 1 nA Na^+ current for 1 ms causes 1 nA × 1 ms/~10 pL = 1 pC/~10 pL = ~1.0/10 F mol/L = ~1.0 μM increase in the intracellular Na^+ concentration, where F = ~0.96 × 10^5 C/mol is the Faraday constant.

In order to investigate the possible contribution of dynamic change of reversal potential and intra/extracellular ion concentrations, we re-formulated the model to calculate the reversal potential and consider all intracellular and extracellular ion concentration changes. Upon re-formulating the model, intracellular and extracellular Na^+, Ca2$^+$, and K^+ concentrations are calculated. The coefficient of K^+-entry (αK) is estimated under the assumption that the average volume of a single neuron is ~10 pL.[44] The increase in intracellular K^+ concentration caused by K^+ currents was determined as follows: 1 nA K^+ current for 1 ms causes 1 nA × 1 ms/~10 pL = 1 pC/~10 pL = ~1.0/10 F mol/L = ~1.0 μM increase in the intracellular K^+ concentration, where F = ~0.96 × 10^5 C/mol is the Faraday constant. The volume of extracellular space is assumed to be 0.5 times of the neuronal intracellular volume.[45] Therefore, the coefficient of Na^+-exit (α1Na), Ca^{2+}-exit (α1Ca), and K^+-entry (α1K) are twice the value of Na^+-entry (αNa), Ca^{2+}-entry (αCa), and K^+-entry (αK), respectively.

The time course of intracellular and extracellular Na^+ concentration are modeled as follows:
Formulas for the NAN model are given by

$$\frac{d[Na^+]in}{dt} = -\alpha_{Na} A(I_{UNaV} + I_{Na-NALCN}) - \frac{[Na^+]in}{\tau_{Na}} \quad \text{(Equation 99)}$$

$$\frac{d[Na^+]out}{dt} = \alpha 1_{Na} A(I_{UNaV} + I_{Na-NALCN}) + \frac{2[Na^+]in}{\tau_{Na}} \quad \text{(Equation 100)}$$

Formulas for the NAN model with Na^+/K^+ ATPase are given by

$$\frac{d[Na^+]in}{dt} = -\alpha_{Na} A(I_{UNaV} + I_{Na-NALCN} - 3I_{NaK}) \quad \text{(Equation 101)}$$

$$\frac{d[Na^+]out}{dt} = -\alpha 1_{Na} A(I_{UNaV} + I_{Na-NALCN} - 3I_{NaK}) \quad \text{(Equation 102)}$$

Formulas for the FNAN model are given by

$$\frac{d[Na^+]in}{dt} = -\alpha_{Na} A(I_{Na} + I_{NaP} + I_{UNaV} + I_{Na-NALCN}) - \frac{[Na^+]in}{\tau_{Na}} \quad \text{(Equation 103)}$$

$$\frac{d[Na^+]out}{dt} = -\alpha 1_{Na} A(I_{Na} + I_{NaP} + I_{UNaV} + I_{Na-NALCN}) + \frac{2[Na^+]in}{\tau_{Na}} \quad \text{(Equation 104)}$$

The time course of intracellular and extracellular Ca^{2+} concentration are modeled as follows:
Formulas for the NAN model are given by

$$\frac{d[Ca^{2+}]in}{dt} = -\alpha_{Ca} A(I_{CaV} + I_{Ca-NALCN}) - \frac{[Ca^{2+}]in}{\tau_{Ca}} \quad \text{(Equation 105)}$$

$$\frac{d[Ca^{2+}]out}{dt} = \alpha 1_{Ca} A(I_{CaV} + I_{Ca-NALCN}) + \frac{2[Ca^{2+}]in}{\tau_{Ca}} \quad \text{(Equation 106)}$$

Formulas for the NAN model with Na^+/K^+ ATPase are given by

$$\frac{d[Ca^{2+}]in}{dt} = -\alpha_{Ca} A(I_{CaV} + I_{Ca-NALCN}) - \frac{[Ca^{2+}]in}{\tau_{Ca}} \quad \text{(Equation 107)}$$

$$\frac{d[Ca^{2+}]out}{dt} = \alpha 1_{Ca} A(I_{CaV} + I_{Ca-NALCN}) + \frac{2[Ca^{2+}]in}{\tau_{Ca}} \quad \text{(Equation 108)}$$

Formulas for the FNAN model are given by

$$\frac{d[Ca^{2+}]in}{dt} = -\alpha_{Ca} A(I_{CaV} + I_{Ca-NALCN}) - \frac{[Ca^{2+}]in}{\tau_{Ca}} \quad \text{(Equation 109)}$$

$$\frac{d[Ca^{2+}]out}{dt} = \alpha 1_{Ca} A(I_{CaV} + I_{Ca-NALCN}) + \frac{2[Ca^{2+}]in}{\tau_{Ca}} \quad \text{(Equation 110)}$$

The time course of intracellular and extracellular K^+ concentration are modeled as follows:
Formulas for the NAN model are given by

$$\frac{d[K^+]in}{dt} = -\alpha_K A(I_K + I_{LeK} + I_{K-NALCN} + I_{KNa}) - \frac{[K^+]out}{\tau_K} \quad \text{(Equation 111)}$$

$$\frac{d[K^+]out}{dt} = \alpha 1_K A(I_K + I_{LeK} + I_{K-NALCN} + I_{KNa}) + \frac{2[K^+]out}{\tau_K} \quad \text{(Equation 112)}$$

Formulas for the NAN model with Na^+/K^+ ATPase are given by

$$\frac{d[K^+]in}{dt} = -\alpha_K A(I_K + I_{LeK} + I_{K-NALCN} + I_{KNa} + 2I_{NaK}) \quad \text{(Equation 113)}$$

$$\frac{d[K^+]out}{dt} = -\alpha 1_K A(I_K + I_{LeK} + I_{K-NALCN} + I_{KNa} - 2I_{NaK}) \quad \text{(Equation 114)}$$

Formulas for the FNAN model are given by

$$\frac{d[K^+]in}{dt} = -\alpha_K A(I_K + I_{LeK} + I_{K-NALCN} + I_{KNa} + I_A + I_{KS} + I_{KCa}) - \frac{[K^+]out}{\tau_K} \quad \text{(Equation 115)}$$

$$\frac{d[K^+]out}{dt} = -\alpha 1_K A(I_K + I_{LeK} + I_{K-NALCN} + I_{KNa} + I_A + I_{KS} + I_{KCa}) + \frac{2[K^+]out}{\tau_K} \quad \text{(Equation 116)}$$

Reversal potential of Na^+, Ca^{2+}, and K^+ can be calculated as dynamic parameters where R = 8.314472J/(K·mol) is the Gas constant, T = 310K is the temperature, and F = 96485.3399C/mol is the Faraday constant.

$$V_{Na} = 1000\frac{RT}{F}\ln\frac{[Na^+]out}{[Na^+]in} \quad \text{(Equation 117)}$$

$$V_{Ca} = 1000\frac{RT}{2F}\ln\frac{\left[Ca^{2+}\right]out}{\left[Ca^{2+}\right]in} \quad \text{(Equation 118)}$$

$$V_K = 1000\frac{RT}{F}\ln\frac{[K^+]out}{[K^+]in} \quad \text{(Equation 119)}$$

Parameter search

We searched for parameter sets with UDO. The parameter sets are randomly created in a parameter space defined as follows: the conductances of intrinsic
(nonsynaptic) channels in the soma (g_{Leak}, g_{Na}, g_{KNa}, g_{UNaV}, g_K, g_{NaK}, g_{Ca}, g_A, g_{KS}, g_{KCa}, g_{NaP}, g_{AR}) and extrinsic (synaptic) channels in the dendrite (g_{AMPA}, g_{NMDA}, g_{GABA}) were generated by selecting parameters from an exponential distribution bounded to the interval 0.001–10 mS/cm^2; the time constant of Na^+ pumps/exchangers (τ_{Na}) was generated by selecting a parameter from an exponential distribution bounded to the interval 1,000–10,000 ms; the time constant of Ca^{2+} pumps/exchangers (τ_{Ca}) was generated by selecting a parameter from an exponential distribution bounded to the interval 10–1,000 ms; and the shifts of the activation curve (x) and inactivation curve (y) were generated by selecting parameters from a uniform distribution bounded to the interval −45–45 mV. The intervals used in the parameter searches for the conductances of the intrinsic and extrinsic channels were set to be of the same range after consideration of the area of a neuron, A = 0.02 mm^2 (i.e., 0.0002–2 μS/0.002 mm^2 = 0.001–10 mS/cm^2). The procedure of the parameter search was the same as that in the previous study,[11] except for g_{UNaV}, g_{KNa}, g_{NaK}, τ_{Na}, x, and y, which were newly introduced in this study. Differential equations were solved to compute the membrane potential from 0 to 20 s, and odeint function in SciPy was used. The simulated time course of the membrane potential from 10 to 20 s was specifically used to analyze the wave pattern of the membrane potential. This interval was selected to exclude the influence of the initial conditions of the differential equations on the observed wave pattern. The procedure of the wave-type classification was the same as that in the previous study.[11] The major frequency of the oscillatory behavior was then analyzed via fast Fourier transform (FFT) by using the periodogram function in the SciPy library. Furthermore, the fine structure of the wave pattern was evaluated by counting the number of spikes per 1 s, and the number of spikes was determined as half the number of times the membrane potential crossed −20 mV. Solutions, in which the membrane potential exceeded this threshold at almost all time points (>95%), were eliminated at this point (labeled as "ELSE"). Based on these characteristics, the solutions were classified into four categories: "RESTING" (spike numbers per second <2 or peak frequency = 0 Hz), "UDO" (0 Hz < peak frequency <10 Hz and spike number per second >5 × peak frequency), "AWAKE" (peak frequency ≥10 Hz), and "UDO with few spikes" (0 Hz peak frequency <10 Hz and spike number per second <5 × peak frequency). "UDO with few spikes" indicated that the solution exhibited a slow-wave activity, with fewer than five spikes during one bursting phase of neural activity. All of the solutions classified as "UDO" were then manually checked to select the ones that exhibited oscillatory membrane potential alternating between the bursting and silent phases.

Bifurcation analysis

To analyze the behavior of the system around the parameter set that induced UDO, we conducted bifurcation analyses. Each conductance or the time constant was gradually changed from 0.01 to 100 times its original value; for x and y, the gradual changes ranged from −45 to +45 of the original value. The solutions were then classified into four categories, namely, RESTING, UDO, AWAKE, and ELSE, as aforementioned. In the bifurcation analysis, the "UDO" components included both "UDO" and "UDO with few spikes." Manual curation of the classification was not conducted for the result of the bifurcation analysis.

Plotting the normalized voltage (V) and [Na^+]

To see the association between the V and [Na^+] time courses, we plotted the time course for all parameter sets inducing UDO. For V, the maximum voltage was expressed by 3 and the minimum by −3. For [Na^+], the maximum concentration was expressed by 3 and the minimum by −3. The period of each oscillation was standardized for all parameter sets and plotted.

Choosing the representative parameter set

PCA was conducted to the parameter with ∼1,000 UDO. Subsequently, the probability density function was calculated for PC1 and PC2 based on the kernel density estimation using the PCA function in the scikit-learn library. 100 parameter sets were selected according to the probability density (top 100), and the representative parameter set was chosen arbitrarily from these parameter sets.

Plotting the intersection of nullplanes

The NAN model consisted of ODEs with four variables (V, n_K, h_{UNaV}, Na^+). By fixing the value of the intracellular Na^+, it can be converted to ODEs with three variables (V, n_K, h_{UNaV}). Using $\frac{dV}{dt}$ described in 8 and $\frac{dh_{UNaV}}{dt}$ described in 29, the intersection of the V, h_{UNaV}

null planes satisfies $\frac{dV}{dt} = 0$ and $\frac{dh_{UNaV}}{dt} = 0$ given by the following equations:

$$\frac{dV}{dt} = 0 \quad \text{(Equation 120)}$$

$$\Leftrightarrow \frac{1}{C}(I_{Leak} + I_K + I_{UNaV} + I_{KNa} + I_{Ca}) = 0 \quad \text{(Equation 121)}$$

$$\Leftrightarrow I_{UNaV} = -(I_{Leak} + I_K + I_{KNa} + I_{Ca}) \quad \text{(Equation 122)}$$

$$\Leftrightarrow g_{UNaV} m_{UNaV}{}^3 h_{UNaV}(V - V_{Na}) = -\{g_{Leak}(V - V_{Leak}) + g_K n_K{}^4(V - V_K) + g_{KNa} m_{KNa}(V - V_K) + g_{Ca} m_{Ca}{}^2(V - V_{Ca})\} \quad \text{(Equation 123)}$$

$$\Leftrightarrow h_{UNaV} = -\frac{g_{Leak}(V - V_{Leak}) + g_K n_K{}^4(V - V_K) + g_{KNa} m_{KNa}(V - V_K) + g_{Ca} m_{Ca}{}^2(V - V_{Ca})}{g_{UNaV} m_{UNaV}{}^3(V - V_{Na})} \quad \text{(Equation 124)}$$

$$m_{KNa} = 1 \Big/ \left[1 + (Ke/[Na^+])^{Kf}\right] \quad \text{(Equation 125)}$$

$$m_{Ca} = 1/[1 + exp(-(V + 20)/9)] \quad \text{(Equation 126)}$$

$$m_{UNaV} = \alpha_m / (\alpha_m + \beta_m) \quad \text{(Equation 127)}$$

$$\alpha_m = 0.1(V + 33 + x)/[1 - exp(-(V + 33 + x)/10] \quad \text{(Equation 128)}$$

$$\beta_m = 4\, exp(-(V + 53.7 + x)/12) \quad \text{(Equation 129)}$$

$$\frac{dh_{UNaV}}{dt} = 0 \quad \text{(Equation 130)}$$

$$\Leftrightarrow 4(\alpha_h(1 - h_{UNaV}) - \beta_h h_{UNaV}) = 0 \quad \text{(Equation 131)}$$

$$\Leftrightarrow (\alpha_h + \beta_h) h_{UNaV} = \alpha_h \quad \text{(Equation 132)}$$

$$\Leftrightarrow h_{UNaV} = \frac{\alpha_h}{(\alpha_h + \beta_h)} \quad \text{(Equation 133)}$$

$$\alpha_h = 0.07\, exp(-(V + 50 + y)/10) \quad \text{(Equation 134)}$$

$$\beta_h = 1/[1 + exp(-(V + 20 + y)/10)] \quad \text{(Equation 135)}$$

Therefore, if the value of the membrane voltage (V) is determined, the values of n_K and h_{UNaV} are calculated as follows.

$$h_{UNaV} = \frac{\alpha_h}{(\alpha_h + \beta_h)} \quad \text{(Equation 136)}$$

n_K satisfies the following equation.

$$\frac{\alpha_h}{(\alpha_h + \beta_h)} = -\frac{g_{Leak}(V - V_{Leak}) + g_K n_K{}^4(V - V_K) + g_{KNa} m_{KNa}(V - V_K) + g_{Ca} m_{Ca}{}^2(V - V_{Ca})}{g_{UNaV} m_{UNaV}{}^3(V - V_{Na})} \quad \text{(Equation 137)}$$

$$\Leftrightarrow \frac{\alpha_h g_{UNaV} m_{UNaV}{}^3(V - V_{Na})}{(\alpha_h + \beta_h)} = -\{g_{Leak}(V - V_{Leak}) + g_K n_K{}^4(V - V_K) + g_{KNa} m_{KNa}(V - V_K) + g_{Ca} m_{Ca}{}^2(V - V_{Ca})\} \quad \text{(Equation 138)}$$

$$\Leftrightarrow g_K {n_K}^4 (V - V_K) = -\left\{\frac{\alpha_h g_{UNaV} {m_{UNaV}}^3 (V - V_{Na})}{(\alpha_h+\beta_h)} + g_{Leak}(V - V_{Leak}) + g_{KNa} m_{KNa} (V - V_K) + g_{Ca} {m_{Ca}}^2 (V - V_{Ca})\right\} \quad \text{(Equation 139)}$$

$$\Leftrightarrow {n_K}^4 = -\left\{\frac{\alpha_h g_{UNaV} {m_{UNaV}}^3 (V - V_{Na})}{(\alpha_h+\beta_h)} + g_{Leak}(V - V_{Leak}) + g_{KNa} m_{KNa} (V - V_K) + g_{Ca} {m_{Ca}}^2 (V - V_{Ca})\right\} \Big/ g_K (V - V_K) \quad \text{(Equation 140)}$$

Therefore,

$$n_K = \left[-\left\{\frac{\alpha_h g_{UNaV} {m_{UNaV}}^3 (V - V_{Na})}{(\alpha_h+\beta_h)} + g_{Leak}(V - V_{Leak}) + g_{KNa} m_{KNa} (V - V_K) + g_{Ca} {m_{Ca}}^2 (V - V_{Ca})\right\} \Big/ g_K (V - V_K)\right]^{0.25} \quad \text{(Equation 141)}$$

Using $\frac{dh_{UNaV}}{dt}$ described in 29 and $\frac{dn_K}{dt}$ described in 18, the intersection of n_K, h_{UNaV} null planes is the line that satisfies $\frac{dn_K}{dt} = 0$ and $\frac{dh_{UNaV}}{dt} = 0$.

$$\frac{dh_{UNaV}}{dt} = 0 \quad \text{(Equation 142)}$$

$$\Leftrightarrow 4\left(\alpha_h (1 - h_{UNaV}) - \beta_h h_{UNaV}\right) = 0 \quad \text{(Equation 143)}$$

$$\Leftrightarrow (\alpha_h+\beta_h) h_{UNaV} = \alpha_h \quad \text{(Equation 144)}$$

$$\Leftrightarrow h_{UNaV} = \frac{\alpha_h}{(\alpha_h+\beta_h)} \quad \text{(Equation 145)}$$

$$\alpha_h = 0.07\, exp\left(-(V + 50 + y)/10\right) \quad \text{(Equation 146)}$$

$$\beta_h = 1/\left[1 + exp\left(-(V + 20 + y)/10\right)\right] \quad \text{(Equation 147)}$$

$$\frac{dn_K}{dt} = 0 \quad \text{(Equation 148)}$$

$$\Leftrightarrow 4(\alpha_n(1 - n_K) - \beta_n n_K) = 0 \quad \text{(Equation 149)}$$

$$\Leftrightarrow n_K = \frac{\alpha_n}{\alpha_n+\beta_n} \quad \text{(Equation 150)}$$

$$\alpha_n = 0.01(V + 349/\left[1 - exp(-(V + 34)/10\right] \quad \text{(Equation 151)}$$

$$\beta_n = 0.125\, exp\left(-(V + 44)/25\right) \quad \text{(Equation 152)}$$

Therefore, if the value of the membrane voltage (V) is determined, the values of n_K and h_{UNaV} are calculated as follows:

$$h_{UNaV} = \frac{\alpha_h}{(\alpha_h+\beta_h)} \quad \text{(Equation 153)}$$

$$n_K = \frac{\alpha_n}{\alpha_n+\beta_n} \quad \text{(Equation 154)}$$

Measuring the up-state duration, down-state duration, Na^+ oscillation amplitude, and ISI

The duration of the up and down states is determined as follows (Figure S3A). In a two-dimensional plane where the x axis represents time (t) and the y axis represents the membrane potential (V), V = f(t). The time course of the membrane potential is given by V = f(t).

First, through FFT analysis on the V = f(t) time series data, the frequency of UDO was determined as the frequency *fq* (Hz) with the highest power (Figure S3A).

Then, the number of intersection points between V = f(t) and V = k (k increased from −110 to 40 mV in increments of 0.1 mV) was computed. If the value of k was small, the intersection points would lie in the down state (Figure S3B). By gradually increasing the value of k, the intersection points shifted toward the up state, where the number of intersection points would be abruptly increased (Figure S3C). Hence, by examining the association between the value of k and the number of intersection points, the membrane potential, at which the transition between the up and down states occurs, can be estimated as the k value with an acute increase in the intersection points. The detailed algorithm was implemented as follows.

We defined the threshold value of k = k_{thresh} as the up-state membrane voltage close to the boundary in the transition between the up and down states. k_{thresh} was calculated as follows: as the value of k increased from −110 mV in increments of 0.1 mV, the number of the intersection point gradually increased. Then, after the number of the intersection point exceeded $30 \times 2 \times fq + 100$, the value of k was determined as k_{thresh}. This was because $30 \times 2 \times fq$ matched the up-to-down-state transition timing during the simulated time of 30 s, and the addition of 100 ensured the marked increase in the intersection points within the up state.

Next, among all the intersection points between V = f(t) and V = k_{thresh}, those accounting for the transition from the down to the up state or from the up to the down state were selected. The t coordinate of intersection points was defined as t_{int} (msec) and determined as follows:

$$f(t_{int} + j) = \begin{cases} < k_{thresh} \begin{cases} (-30 \le j \le -1 : \text{from the down state to the up state}) \\ (1 \le j \le 30 : \text{from the up state to the down state}) \end{cases} \\ \le k_{thresh} \begin{cases} (j = 0 : \text{from the down state to the up state}) \\ (j = 0 : \text{from the up state to the down state}) \end{cases} \\ > k_{thresh} \begin{cases} (1 \le j \le 2 : \text{from the down state to the up state}) \\ (-2 \le j \le -1 : \text{from the up state to the down state}) \end{cases} \end{cases} \quad \text{(Equation 155)}$$

The transition points between the up and down states were determined as above because at the transition point from the down to the up state, f(t) was constantly below k_{thresh} when $t_{int} < t$ and only after t exceeds t_{int}, f(t) is larger than k_{thresh} because during the down state membrane potential is hyperpolarized and only when it is in the up-state period membrane potential surpasses the threshold voltage (Figure S3D). The same logic was applied when determining the transition point from the up to the down state (Figure S3E).

Using the transition time between the up and the down states, the up- and down-state period was calculated. The periods were calculated for many cycles of oscillation; thus, the average period of the up and down states was calculated.

The Na^+ oscillation amplitude was calculated for many cycles of oscillation; thus, the average value was calculated.

To calculate the ISI, all local maximum points were first extracted from the time-series data of V = f(t) using the argrelmax function in the SciPy library. ISI is defined as the interval between adjacent local maximum points. However, an ISI exceeding 60 msec is excluded because an ISI that is too long can be confused with the short down state. ISI accounting for all adjacent spikes are calculated individually, and the average value is obtained.

Construction of the network model

A network model consisting of 84 neurons was constructed. The parameters (i.e., conductance of ion channels and synaptic receptors) were homogeneous throughout all the neurons in one network model. Each neuron was randomly connected to the other neurons with a probability of 20% by AMPA- and NMDA-mediated synapses. Of all the 2,137 parameter sets with UDO in the FNAN model, 1703 exhibited UDO in the FNAN model where $g_{GABA} = 0$. Among them, we chose 1,057 parameter sets with UDO in the FNAN model, which were confirmed by calculation using a fourth-order Runge–Kutta method with a time step of 0.1 msec. Finally, 100 of the 1,057 parameter sets were chosen as representative sets. The selection method for the representative parameter sets was the same as that in the analysis using an AN model with a mean-field approximation.

Simulations were performed using GPU (NVIDIA GeForce RTX 3090), and numerical calculations were conducted using the fourth-order Runge–Kutta method with a time step of 0.01 msec. Codes are written using CUDA.

QUANTIFICATION AND STATISTICAL ANALYSIS

Figures represent averaged or representative results of multiple independent simulations. The figure legends provide details concerning the simulations.